Stably Stratified Turbulence

1 Introduction

Consider a flow with a stable mean density stratification,

$$N^2(z) \;=\; \frac{d\bar{b}}{dz}(z) \;>\; 0\,. \tag{1}$$

Here, as usual, the vertical coordinate is in the opposite direction to the gravitational force. An important regime parameter is the *gradient Richardson number*,

$$Ri \;=\; N^2 \Big/ \left(\frac{\partial \overline{\mathbf{u}}_h}{\partial z}\right)^2 , \tag{2}$$

where the subscript h denotes the horizontal component. Ri measures both the gravitational stability of the stratification and the dynamical competition with the mean shear. When $Ri < 0$, the flow will be in a state of convective turbulence for $Re, Ra \gg 1$, with possibly some influences by the mean shear if it is strong enough. When $0 \le Ri \le \mathcal{O}(1)$, the flow will be a type shear turbulence (*e.g.,* as in the Kelvin-Helmholtz flow) for $Re \gg 1$, with some modification by the weakly stable stratification. However, when $Ri \gg 1$, the turbulence is different from either of these regimes and is referred to as *stratified turbulence* when $Re \gg 1$. Because the influence of the stratification is strong in this latter regime, its motions are anisotropic, $w \;\ll\; u, v$, because of the large gravitational work required for vertical movement. The behavior of stratified turbulence is in contrast to weakly nonlinear internal wave "turbulence," which is also consistent with $Ri,\; Re \;\gg\; 1$ (Sec. 2). In nature, away from boundary layers, Ri is usually $\gg 1$, and both turbulence and wave regimes occur. There remains considerable uncertainty about the proportional occurrences of each type of dynamics. In the *2D Homogeneous Turbulence* chapter, a measured wavenumber spectrum was shown for the atmospheric mesoscale. How much of the observed regime with $E_h(k) \;\propto\; k^{-5/3}$ is due to stratified turbulence and how much is due to internal waves? And can the portion attributable to stratified turbulence be understood as a manifestation of 2D inverse energy cascade (Sec. 5)?

Stratified turbulence does not have an obvious energy source from a local instability of its environment: since $N^2 > 0$, the flow is gravitationally stable, and since $Ri > \mathcal{O}(1)$ the flow is Kelvin-Helmholtz stable. Thus, either this regime is one of decaying turbulence or else it must be sustained by an energy cascade from some other phenomenon — such as a forward cascade from geostrophic turbulence, inertial and internal gravity waves generated elsewhere that break locally in the interior, or an inverse energy cascade from atmospheric convection.

Geostrophic turbulence is most likely to be energetically sustained by the rotating shear instability of large-scale winds and currents, either climatological or transient. Its standard (*i.e.,* quasigeostrophic) model exhibits an inverse energy cascade, analogous to 2D turbulence, which implies a lack of energization for the smaller-scale stratified regime with $Fr \ll 1$ and $Ro \gg 1$. Furthermore, there are plausible theoretical arguments why stratified turbulence might itself exhibit an inverse energy cascade (Sec. 2). Nevertheless, there is increasing evidence that forward energy cascades usually occur from larger scales into the stratified turbulence regime and continue down to Kolmogorov universality and microscale dissipation (Sec. 5 and *Geostrophic Turbulence*).

In most locations inertial or internal gravity waves are energetically sustained by propagation from some remote source, usually located at the vertical boundary and due either to tidal or sub-tidal flow past topography or to fluctuating boundary stress. Internal waves also can be generated by convective buoyancy flows, such as gravity currents or cumulus clouds, and even by stably stratified planetary boundary layers. If the waves are strong enough to intermittently break and overturn, then a local, more isotropic cascade to dissipation will occur.

It is an important — and until recently partially open — question whether stratified turbulence satisfies the H1 hypothesis of 3D isotropic, homogeneous turbulence, *i.e.,* whether g becomes negligible on sufficiently small scales, but still larger than the dissipation (Kolmogorov) scale. The implication of that this is false is that stratified turbulence would remain anisotropic throughout its cascade to dissipation and — in combination with an expectation of an inverse energy cascade — even have a conundrum about how its dissipation is accomplished. Most previous evidence favored violation of the H1 hypothesis in situations where stratified advective dynamics is more important than internal wave dynamics; however, most of this laboratory and computational evidence is from situations where Re values are not too large (Secs. 2-3). More recent computational evidence supports H1 at large enough Re (Sec. 5).

2 Internal Waves and Vortical Motions

In terms of characteristic scales, we can write Ri in in relation to the previously introduced Froude number, Fr,

$$Ri \sim N^2H^2/V^2 = Fr^{-2} . \tag{3}$$

(Commonly $Ri(\mathbf{x})$ is viewed as a local measure of the stratification and shear influences, while Fr is viewed as a bulk measure.) Thus, stratified turbulence occurs when $Fr \ll 1$, and we can develop an asymptotic dynamical approximation as $Fr \to 0$ (Lilly, 1983; McWilliams, 1985). We distinguish this regime from geostrophic turbulence (also with $Fr \ll 1$) by neglecting rotational influences, *i.e.,* assuming $Ro \gg 1$. Consider a non-dimensionalization of the governing equations by the following advective scales for the stratified turbulence:

$$\begin{aligned} \mathbf{x} \sim H, \quad \mathbf{u}_h \sim V, \quad t \sim H/V \\ \phi \sim V^2, \quad b \sim V^2/H, \quad w \sim V^3/N^2H^2 . \end{aligned} \tag{4}$$

The resulting non-dimensional Boussinesq equations are

$$\begin{aligned} \frac{D_h\mathbf{u}_h}{Dt} + Fr^2 w\frac{\partial \mathbf{u}_h}{\partial z} &= -\nabla_h\phi + \nu\nabla^2\mathbf{u}_h \\ Fr^2\frac{Dw}{Dt} &= -\frac{\partial\phi}{\partial z} + b \\ \frac{D_h b}{Dt} + Fr^2 w\frac{\partial b}{\partial z} + w &= \kappa\nabla^2 b \\ \nabla_h\cdot\mathbf{u}_h + Fr^2\frac{\partial w}{\partial z} &= 0 . \end{aligned} \tag{5}$$

(Here we have retained the diffusive terms, even though we have not made their non-dimensionalization scaling explicit; a more familiar non-dimensional form would have Re^{-1} in place of ν.)

The limiting form for these as $Fr \rightarrow 0$ is a form of 2D dynamics for $\mathbf{u}_h = \hat{\mathbf{z}} \times \nabla_h \psi$ and ϕ, where the flow has only a parametric dependence on z; diagnostic relations for b and w from the second and third equations in (5)[1] ; and a diagnostic relation for the additional $\mathcal{O}(Fr^2)$, horizontally divergent component of the horizontal flow, $\mathbf{u}_h = Fr^2 \nabla_h \chi$, from the fourth equation in (5). Here we are using a Helmholtz decomposition of the 3D non-divergent velocity field,

$$u = -\partial_y \psi + \partial_x \chi \,, \quad v = \partial_x \psi + \partial_y \chi \,, \quad w = -\int^z [\partial_x^2 \chi + \partial_y^2 \chi] \, dz \,. \tag{6}$$

Thus, when $\chi \ll \psi$, the flow is primarily horizontal (as in the example in *Turbulent Flows*), and it can be called *rotational* or *vortical* for its vertical vorticity. In contrast, when $\chi \gg \psi$, the horizontal flow is divergent, and the degree of velocity anisotropy may not be so pronounced.

To leading order in Fr, the dynamics of stratified turbulence is equivalent to the dynamics of 2D turbulence, with an independent evolution of $\mathbf{u}_h$ at each vertical level. This is sometimes called *layerwise 2D turbulence*. Because of sensitive dependence, however, we expect these independent evolutions to diverge, and this should act to decrease the vertical correlation scale and increase vertical shear, with the ultimate effect of somehow coupling the evolutions at different levels and bringing in some higher-order corrections in (5). One set of approximate equations with such behavior results from carrying the asymptotic analysis through $\mathcal{O}(Fr^2)$: the set is called the non-rotating *Balance Equations*, where the horizontal momentum equation in (5) is replaced by approximate forms of its curl and divergence equations (*i.e.,* the vertical vorticity equation and gradient-wind balance); the vertical momentum balance is hydrostatic; and the last two equations in (5) are kept in their entity. The Balance Equations contain vortex-stretching terms that couple the vertical vorticity evolution at different levels, although they have not yet been solved for stratified turbulence and so we cannot yet be sure that they are accurate here, although they are known to be quite accurate for the advective evolution of rotating, stably stratified flows where $Ro = \mathcal{O}(1)$. The Balance Equations are also a first-order PDE system. Balance Equations suitability remains an open question for non-rotating flows for at least three reasons: (1) they are not uniformly valid at $\mathcal{O}(Fr^2)$ because they drop the vertical acceleration term in (5) that is formally of this order; (2) there are flow-dependent solvability conditions for their time integrability (McWilliams *et al.*, 1998) that are more likely to be problematic without rotation than with it; and (3) recent solutions at small Fr and large Re indicate that there may be a partial turbulent Boussinesq solution that exhibits small-scale overturning in a way that is inconsistent with Ri being everywhere large (Sec. 5 below). In summary, the Balance Equations are commonly very accurate on larger, nearly geostrophic scales (*e.g.,* synoptic and meosscale), but probably is most useful as an interpretive framework for some non-rotating, stratified phenomena (*e.g.,* the pancake vortices in Sec. 3) rather than a uniformly valid approximation for all the non-wave behaviors.

Métais and Herring (1989) computationally solved the Boussinesq equations for $Fr(0) \ll 1$ and approximately balanced initial conditions with $\psi \gg \chi$. In the subsequent evolution, $Fr(t)$

[1]The third equation contains a time-derivative in it, so it appears to be undetermined as a diagnostic relation for w. However, this appearance is illusory, since the time derivative for b cannot advance independently of the time derivative of ψ. Thus, the reduced system of (5) with $Fr \rightarrow 0$ is a first order PDE system in time. It is often a subtle matter to correctly identify the temporal order of a PDE system. As another example of the subtlety of this type of assessment, consider that the full Boussinesq system (5) and its hydrostatic approximation, the Primitive Equations. In spite of the occurrence of four time derivatives in the former (*i.e.,* for u, v, w, b) and only three time derivatives for the latter (since Dw/Dt has been dropped), both systems are really third-order in time.

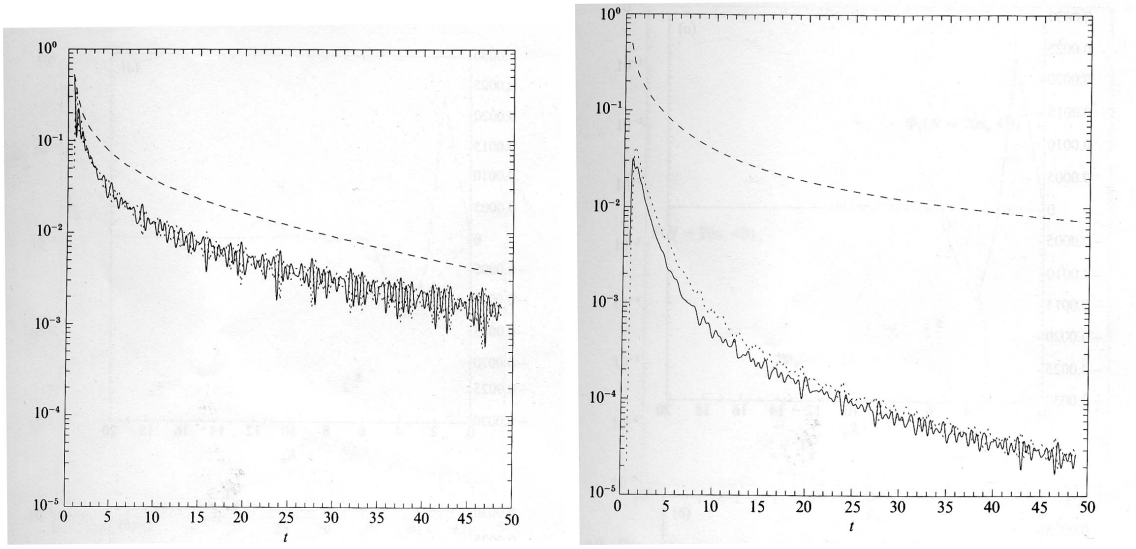

Figure 1: Rotational kinetic energy (dashed line), divergent kinetic energy (solid line), and fluctuation potential energy (dotted line) in freely evolving stratified turbulence. (Left) Isotropic initial conditions for velocity; (Right) Rotational velocity initial conditions. (Métais and Herring, 1989)

remains small and $Fr^4\overline{(\nabla_h\chi)^2} \ll \overline{(\nabla_h\psi)^2}$ continues to hold (Fig. 1, right panel); whereas, with more general initial conditions the ratio between ψ and χ remains $\mathcal{O}(1)$ (Fig. 1, left panel). Therefore, we can conclude that the scaling assumptions behind the preceding asymptotic analysis are uniformly valid in time, at least in these solutions and by this global velocity variance measure, hence there is a plausible basis for believing that the dynamics of the Balance Equations may also be accurate. However, the non-rotating Balance Equations develop singularities in certain regions of transition between local vorticity dominance and local strain dominance (McWilliams *et al.*, 1998). Therefore, it must be true that there are some locations where balanced dynamics break down, perhaps to a more locally isotropic cascade to dissipation or to a local generation of internal wave energy (*n.b.,* the internal wave analysis immediately below with $\chi \gg \psi$). Nevertheless, since a global measure of anisotropy is well preserved under evolution (Fig. 1), it must also be true that these breakdown events are modest in frequency and intensity. Given this seemingly contradictory evidence, as well as that from laboratory experiments (Sec. 3), the theoretical understanding of the advective dynamics of stratified turbulence has been viewed as mysterious in many important aspects.

Notice in Fig. 1 that both types of freely evolving turbulence are significantly dissipative. This indicates that a forward energy cascade is occurring — unlike in 2D turbulence — and it suggests an important role for 3D effects on the small scales, either advective or viscous.

We also note that there is another consistent non-dimensionalization for $Fr \ll 1$ that leads to linear internal gravity waves as the leading-order dynamics when $Re \gg 1$:

$$\begin{aligned} \mathbf{x} \sim H, \quad \mathbf{u} \sim V, \quad t \sim 1/N \\ \phi \sim VNH, \quad b \sim VN\,, \end{aligned} \tag{7}$$

whence

$$\begin{aligned} \frac{\partial \mathbf{u}}{\partial t} + \nabla_h \phi - \hat{\mathbf{z}} b &= -Fr\,(\mathbf{u}\cdot\nabla)\mathbf{u} + \nu\nabla^2\mathbf{u} \\ \frac{\partial b}{\partial t} + w &= -Fr\,(\mathbf{u}\cdot\nabla)b + \kappa\nabla^2 b \\ \nabla_h \cdot \mathbf{u}_h + \frac{\partial w}{\partial z} &= 0\,. \end{aligned} \tag{8}$$

Notice that we do not distinguish between the magnitudes of the horizontal and vertical velocity in this scaling choice. Here the nonlinear terms are of $\mathcal{O}(Fr)$ in (8). Yet on an advective time scale — which is $1/Fr$ times the wave time scale in (7) — the nonlinear effects become important, and a *weakly nonlinear wave turbulence* can induce its own type of cascade to dissipation. Sometimes this dissipation is concentrated in local wave-breaking events that certainly are not weakly nonlinear. In wave breaking events, several outcomes are possible: new gravity waves and/or new stratified turbulence may be generated, and/or a 3D Kolmogorov cascade may be initiated.

Thus, the regime of $Ri \gg 1$ is one where there can be either stratified turbulence or internal gravity waves, or both simultaneously, and the present expectation is that their mutual interactions usually are weak both because their nonlinear coupling terms are estimated to be small and because gravity waves can radiate away from a region, leaving behind a balanced state (*i.e.,* a stratified adjustment process, analogous to geostrophic adjustment when f is significant). In this chapter we will pay more attention to the regime of stratified turbulence.

3 Collapse of Isotropic Turbulence in Stratification

There is a classical problem in stratified turbulence that has been the focus of substantial laboratory experimentation: the evolution of initially isotropic 3D turbulence to its "final" state in a stably stratified fluid. This behavior is referred to as the "collapse" of "active" turbulence to its "fossil" state[2], although there is an obvious dynamical-regime chauvinism in these terminologies. Consider a situation where a wire mesh is dragged rapidly through a region in a stratified fluid in a way that locally excites isotropic 3D motions; an alternative means of their generation is by flying an airplane or submarine and examining the resulting wake; yet another is to have a local breaking event for a large-amplitude wave in a stably stratified location. In all cases the sequence is qualitatively as follows: an energetic spatially localized 3D turbulence is generated in an otherwise stably stratified fluid; the 3D turbulence starts a Kolmogorov cascade to dissipation and begins to weaken while also causing a vertical buoyancy flux, $\overline{w'b'} < 0$, by mixing across the mean vertical buoyancy gradient; the environmental stratification begins to suppress vertical velocities by gravitational inhibition, and the buoyancy flux abates; the now anisotropic turbulence either radiates away from the region as internal gravity waves or evolves further in place by developing "pancake" horizontal vortices of finite vertical extent.

I will describe this problem in more detail based on a presentation by Tony Maxworthy (1998) at a workshop on oceanic turbulence. Prof. Maxworthy is an experimentalist who has worked on the collapse problem for many years.

[2]The term fossil implied the end of advective dynamics with its associated forward energy cascade and dissipation, leaving behind residual density and tracer fluctuations that would slowly diffuse away. We now know that this is a false view since horizontal motions remain strong and ε remains large (Fig. 1).

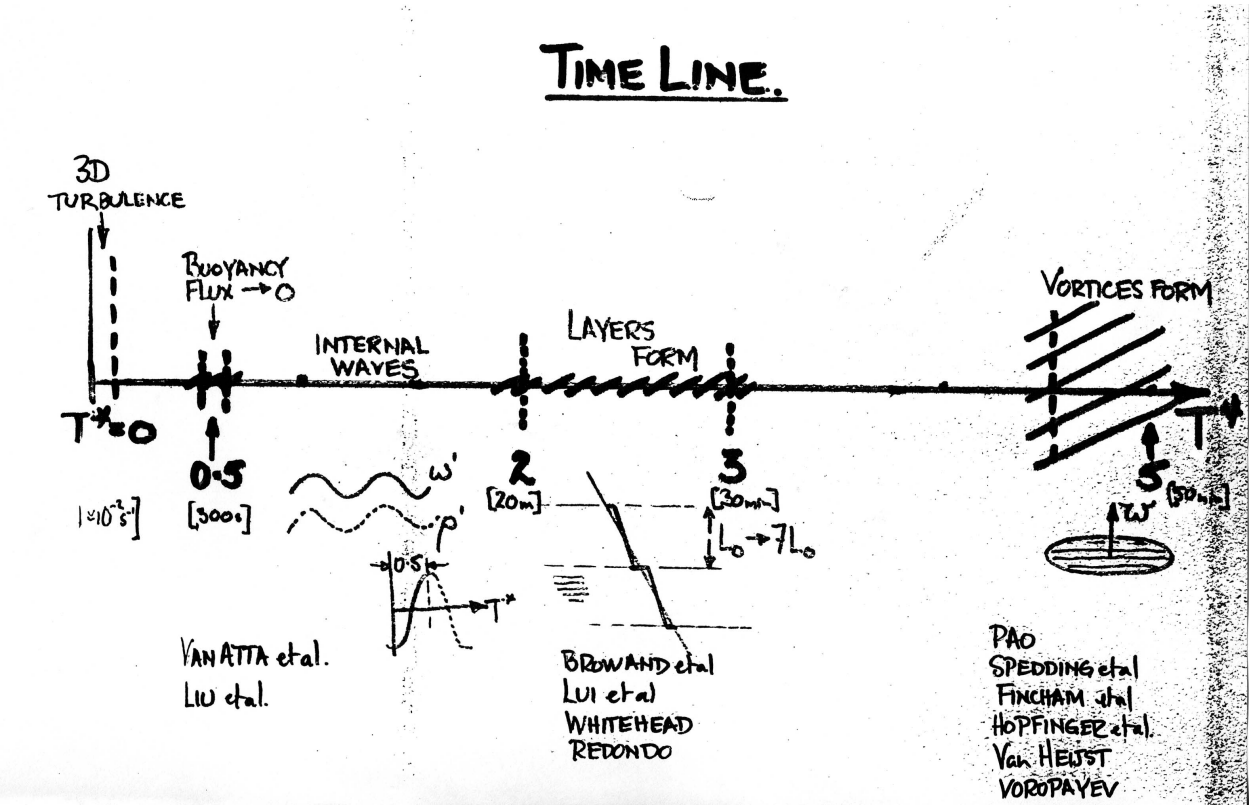

Figure 2: Time line of the evolution of collapsing 3D turbulence in a stratified fluid. (Maxworthy, 1998)

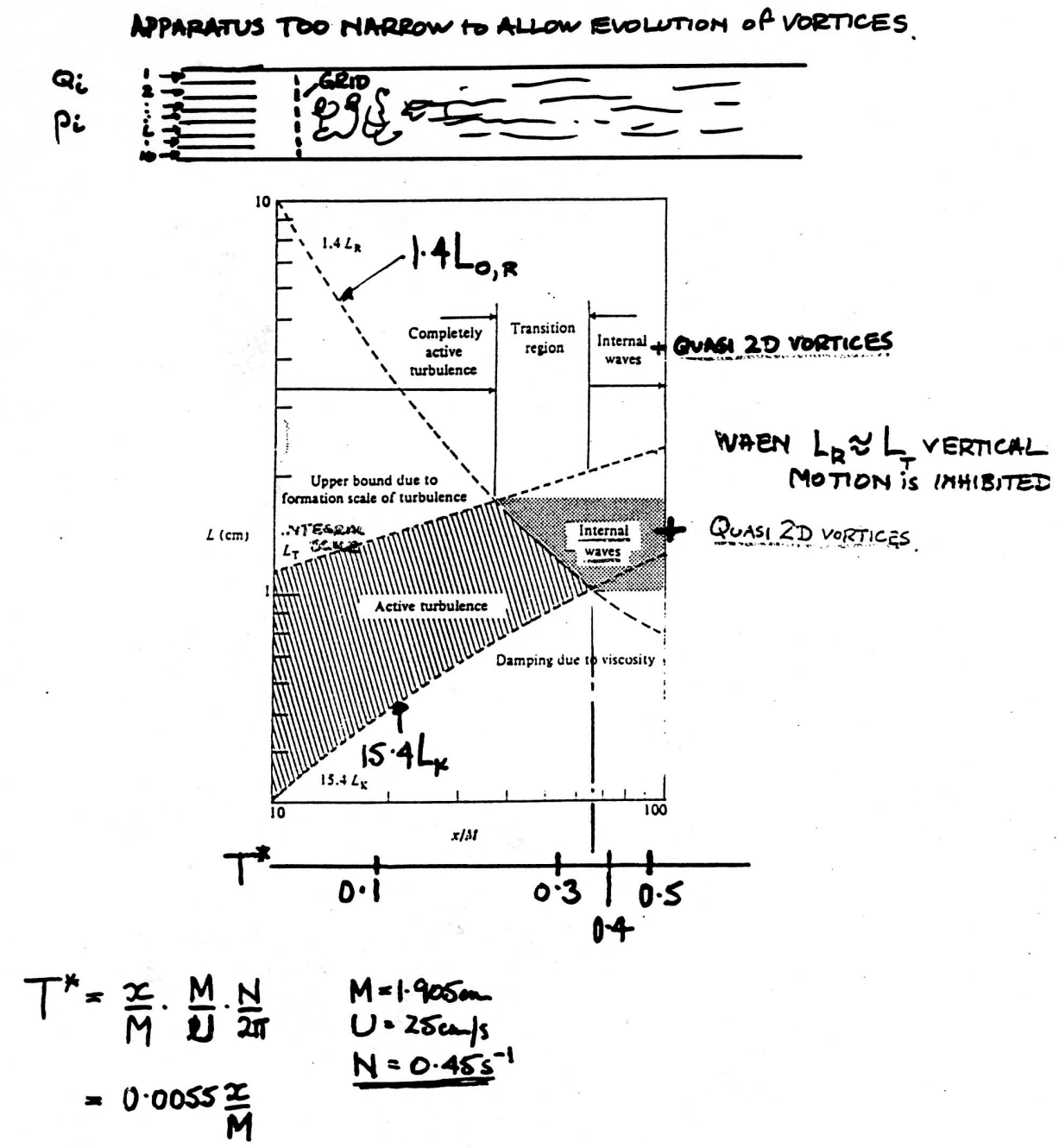

Figure 3: The length scales in collapsing stratified turbulence: Ozmidov scale, L_O, integral scale, L_T, and Kolmogorov scale, $L_K = \eta$. (Stillinger *et al.*, 1983; Maxworthy, 1998)

We define a non-dimensional time,

$$T_* = Nt/2\pi, \tag{9}$$

that we recognize from (4) and (7) as the appropriate non-dimensionalization for gravity waves. Figure 2 provides a summary of the evolutionary sequence. At early times, $0 \leq T_* \leq 0.5$, the 3D turbulence is modified by the ambient stratification, and the vertical buoyancy flux, $\overline{wb}$, is suppressed, after having initially arisen by 3D stirring in the presence of a mean vertical buoyancy gradient. At intermediate times, $0.5 \leq T_* \leq 3.0$, internal waves are generated and propagate away from the turbulent region, and the horizontal layers form that are evident in flow visualizations. These horizontal layers contain anisotropic, advective dynamics, and they expand horizontally to form intrusions into the non-turbulent regions. The vertical scale of these layers when they emerge is approximately the *Ozmidov scale*, L_O, defined by

$$L_O = \sqrt{\varepsilon/N^3}, \tag{10}$$

and with time they grow in thickness to a scale of $\approx 7L_O$ (sometimes called the Pearson-Linden scale). The Ozmidov scale is the marginal scale where 3D overturning motions of a given intensity, hence cascade and dissipation rate, can occur in the presence of a gravitationally inhibiting stratification: for $L < L_O$ (as is initially true for all the 3D turbulent scales), overturning is not strongly inhibited, and for $L > L_O$, it is. Figure 3 shows the evolution of the various length scales. As $L_O(t)$ decreases (because the turbulent energy is decaying and $\varepsilon(t)$ decreases), the turbulent energy peak scale (*e.g.,* the lag-covariance integral scale, $L_T(t)$) grows until L_T becomes larger than L_O. This is a demonstration that there is some degree of inverse energy cascade even in 3D homogeneous turbulence: given energy initially in a narrow wavenumber range, the spectrum breadth will increase to both smaller and larger wavenumbers; the majority of the energy cascades in the forward direction where it is removed by dissipation; this leaves the surviving energy at larger scales on average; hence, L_T increases. These trends continue further until L_O equals the growing Kolmogorov (dissipation) scale,

$$\eta(t) = \left[\nu^3 \Big/ \varepsilon\right]^{1/4} \tag{11}$$

at $T_* \approx 0.5$, and the vertical buoyancy flux, $\overline{w'b'}$, has decreased to approximately zero (Fig. 4). At late times, $T_* \geq 5$, the waves have left the turbulent region, and the remaining turbulence becomes organized into anisotropic coherent vortices, with $w \ll u, v$ and large $|\zeta^{(z)}|$, and a vertical scale like that of the earlier layers. In this stage, the primary contribution to the dissipation rate ε is through the vertical shear of horizontal velocity,

$$\varepsilon \approx \nu \overline{\left(\frac{\partial \mathbf{u}_h}{\partial z}\right)^2} \tag{12}$$

(Fig. 5), that is largest at the top and bottom edges of the coherent vortices. There is no indication that $\varepsilon \to 0$ as $Re \to \infty$ in stratified turbulence. Therefore, this cascade and dissipation route is totally unlike that in 2D turbulence, where ε is entirely due to horizontal velocity shear, $\nabla_h \mathbf{u}_h$, and ε is vanishingly small as $Re \to \infty$. Somehow, though, this vertical kinetic energy cascade

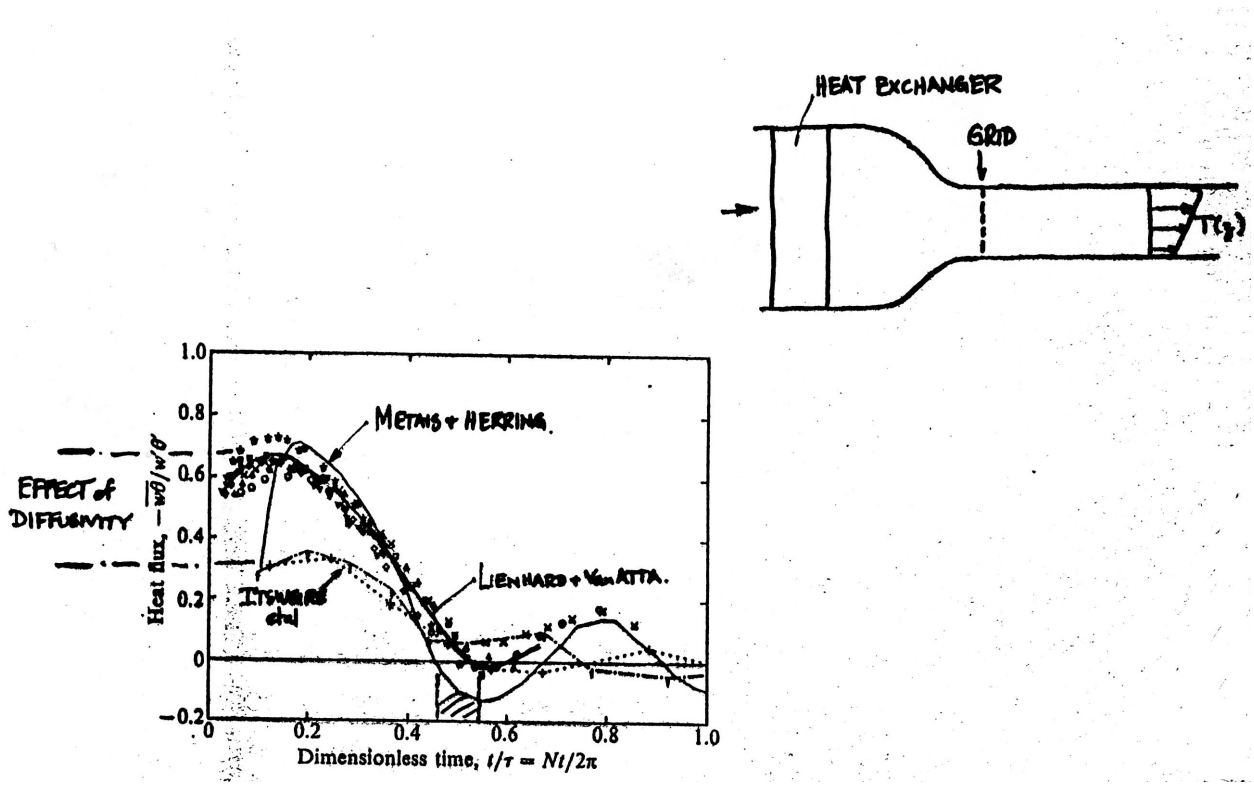

Figure 4: The vertical heat flux in collapsing stratified turbulence for several different values of Pr. (Maxworthy, 1998)

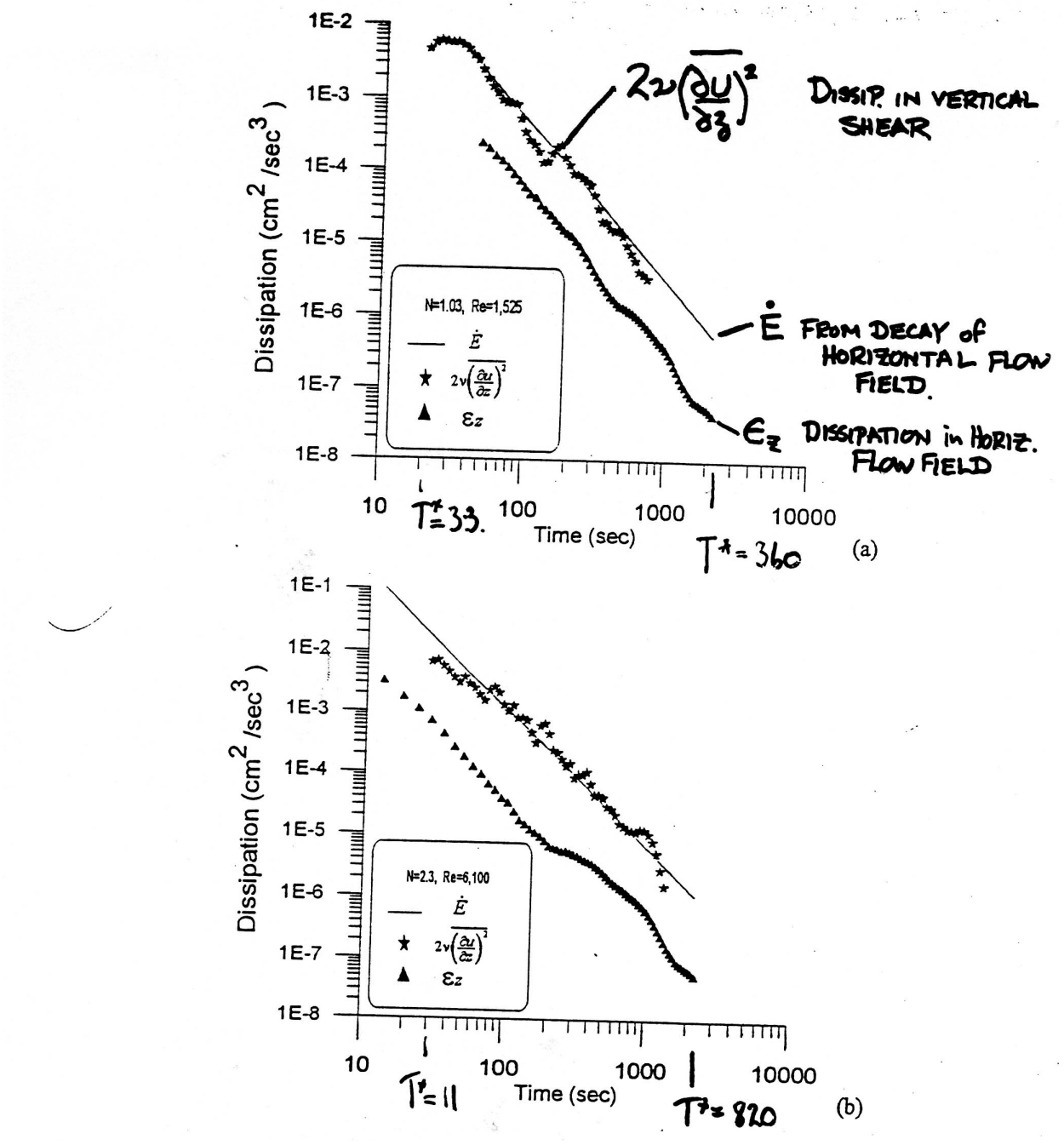

Figure 5: Dissipation in collapsing stratified turbulence over long times. Note that the vertical shear variance accounts for almost all of ε. The symbol ε_z denotes the contribution for dissipation rate from the horizontal shear variance. (Maxworthy, 1998)

coexists with the essentially 2D advective dynamics implicated in the asymptotic scaling analysis in (4)-(5).

This suggests an even simpler approximate model for stratified turbulence with $Fr \ll 1$ than the Balance Equations discussed following (5); *viz.,*

$$\begin{aligned} \frac{D_h \mathbf{u}_h}{Dt} &= -\nabla_h \phi + \nu_v \partial_z^2 \mathbf{u}_h \ \left[+ \nu_h \nabla_h^2 \mathbf{u}_h \right] \\ \nabla_h \cdot \mathbf{u}_h &= 0 \, . \end{aligned} \tag{13}$$

This is equivalent to viscous 2D layerwise dynamics except for the addition of a dominant vertical diffusion term (a similar proposal was made and discussed by Majda & Grote, 1997). As far as I know the 3D system (13) has never been solved, so it remains an open question whether vertical diffusion suffices to control the growth of variance at small horizontal scales that develop during a forward enstrophy cascade (***n.b.,*** this is indicated by the brackets around the ν_h term in (13), raising the possibility that it may be unnecessary in the presence of ν_v). Nevertheless, since Fig. 1 shows the evolutionary consistency of the assumption that $Fr \ll 1$, it remains an open question whether the vertical coupling between different layers occurs only viscously, as in (13), or also through the conservative, vortex-stretching dynamics implicit in the Balance Equations. Even if the latter is the most important mechanism for layer coupling at large Re, it may be that (13) is still a useful representation of this effect if we view ν_v as an eddy viscosity with a larger than molecular magnitude.

Some visualizations of the layers and vortices are shown in Figs. 6-8, and some analyses of the horizontal velocity and both vertical and horizontal vorticity fields during the vortex phase are shown in Fig. 9. The latter clearly show the strong shear, $\partial \mathbf{u}_h / \partial z$, and the associated large horizontal vorticity. The topology of vortex lines is shown in Fig. 10. Computational solutions for stratified turbulence also show that these *pancake vortices* are the dominant coherent structure for this regime (Métais and Herring, 1989). Pancake vortices are somewhat reminiscent of the axisymmetric vortices of 2D turbulence in plan view, but they are spatially much more closely packed in both the vertical and horizontal directions in stratified turbulence.

4 Stratified Shear Layers

In a uniform shear layer, equilibrium turbulence will be established (*Shear Turbulence*, Sec. 1). In a uniformly stratified fluid, initial turbulence will have a transient life cycle and eventually decay toward a stratified rest state, as described in the preceding section. A variant on the latter scenario is a transient life cycle for a stratified shear layer with local vertical shear and buoyancy profiles (*Shear Turbulence*, Sec. 5). It begins as a Kelvin-Helmholtz instability to transverse roll cells, which themselves develop secondary instabilities to spanwise fluctuations. The turbulence intensifies and has vertical eddy mixing of buoyancy and shear that cause the layer to expend vertically and its Richardson number, $Ri = N^2/S^2$, to grow. After the latter exceeds modestly a critical value somewhat larger than 0.25, the truculent energy production shuts off, as does the vertical eddy flux, and the turbulence decays away. A sequence of numerical studies is reported in Smyth and Moum (2000). In particular they analyze the history of several vertical length scales:

- the integral scale, outer scale, or layer thickness (here designated by ℓ_θ instead of L_T as in the preceding figures).

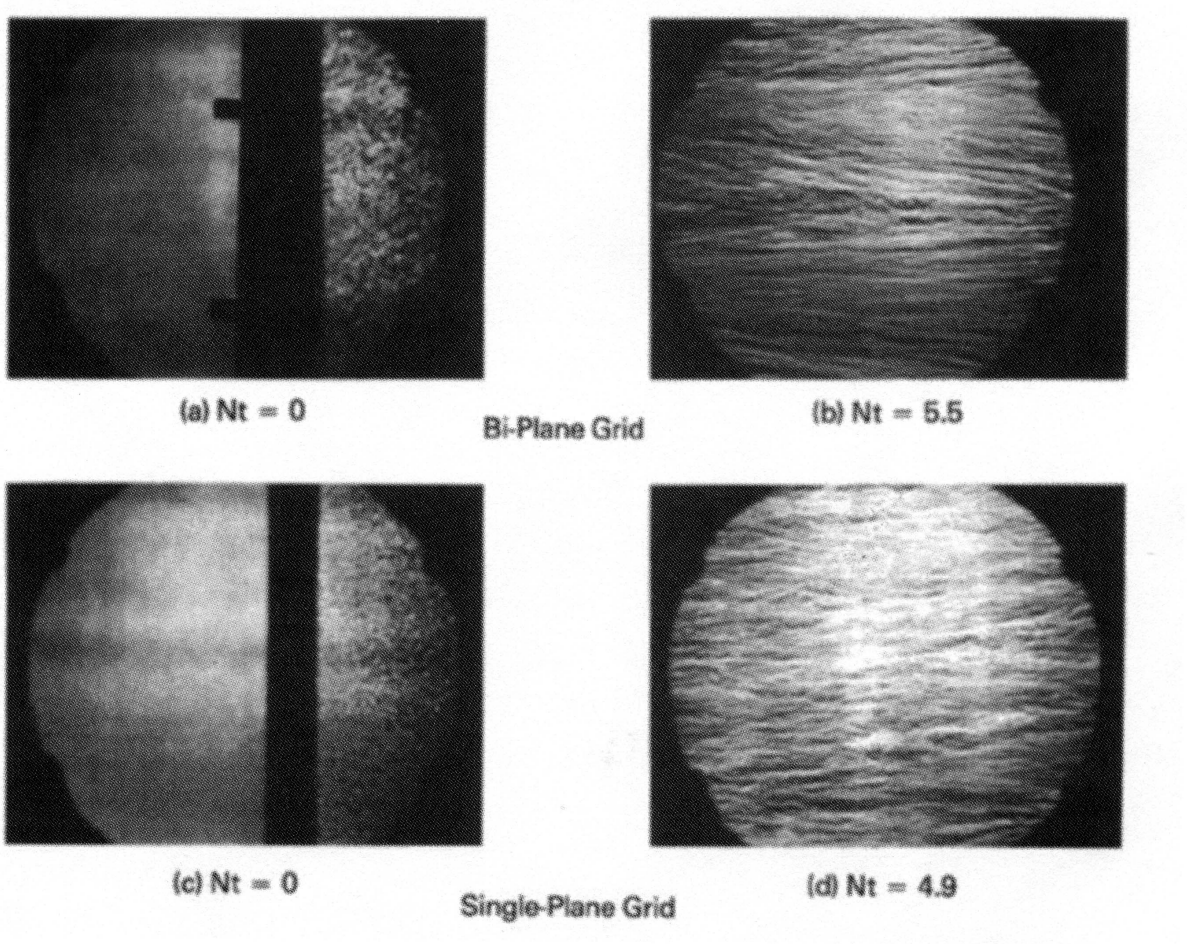

Figure 6: Shadowgraphs of grid-generated turbulence in a stratified fluid, showing the development of density layers when $Nt \gg 1$. (Lin and Pao, 1979)

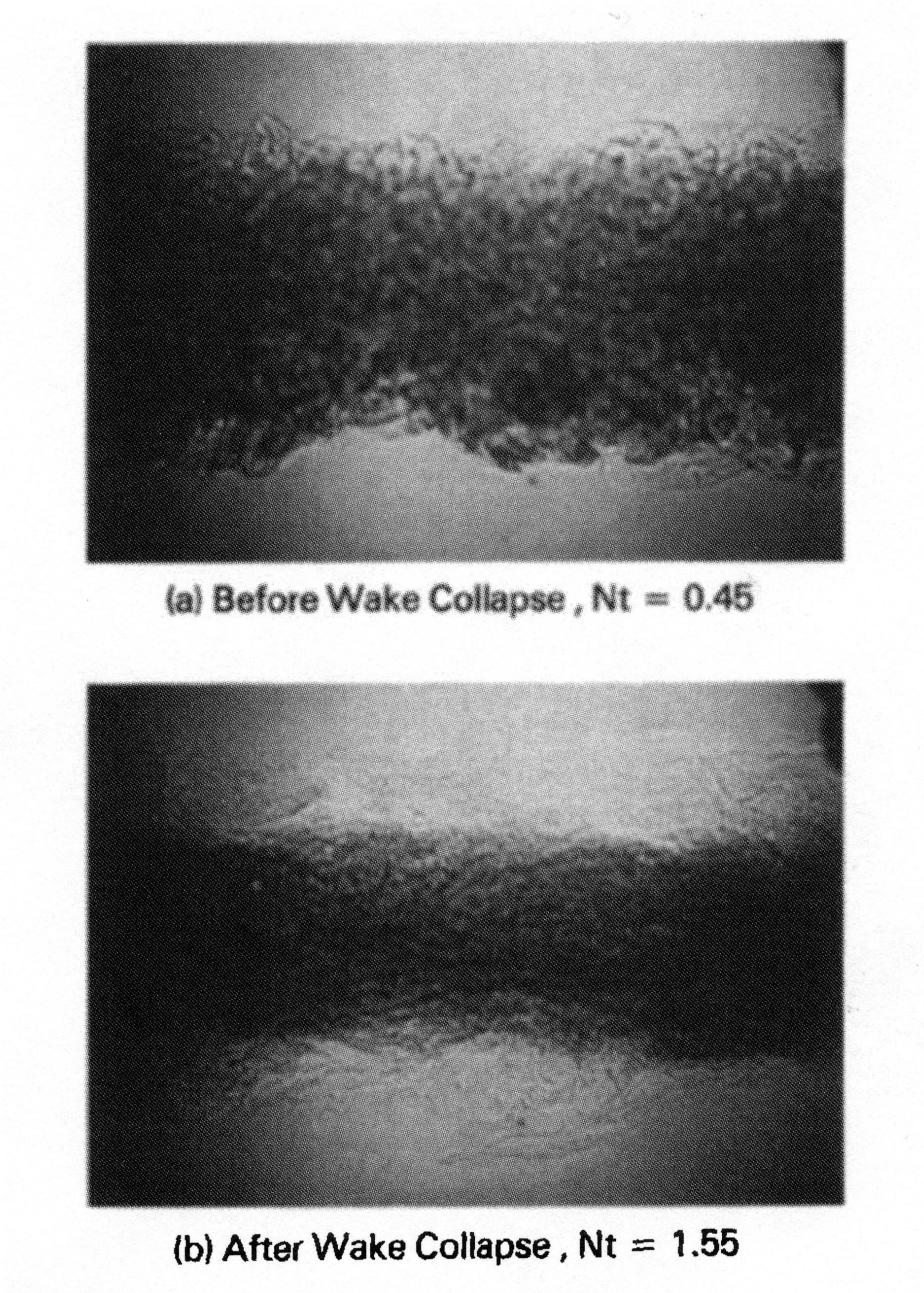

Figure 7: Shadowgraph and dye visualization of the wake of a self-propelled slender body in a stratified fluid, viewed from the side. (Lin and Pao, 1979)

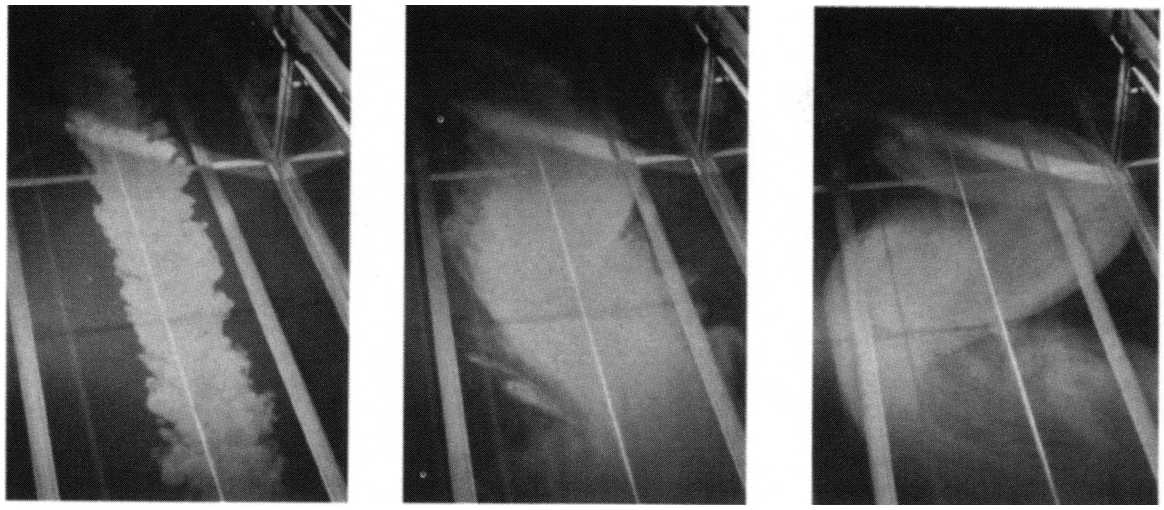

Figure 8: Evolution of pancake vortices in the wake of a towed slender body in a stratified fluid, viewed from the top. (Lin and Pao, 1979)

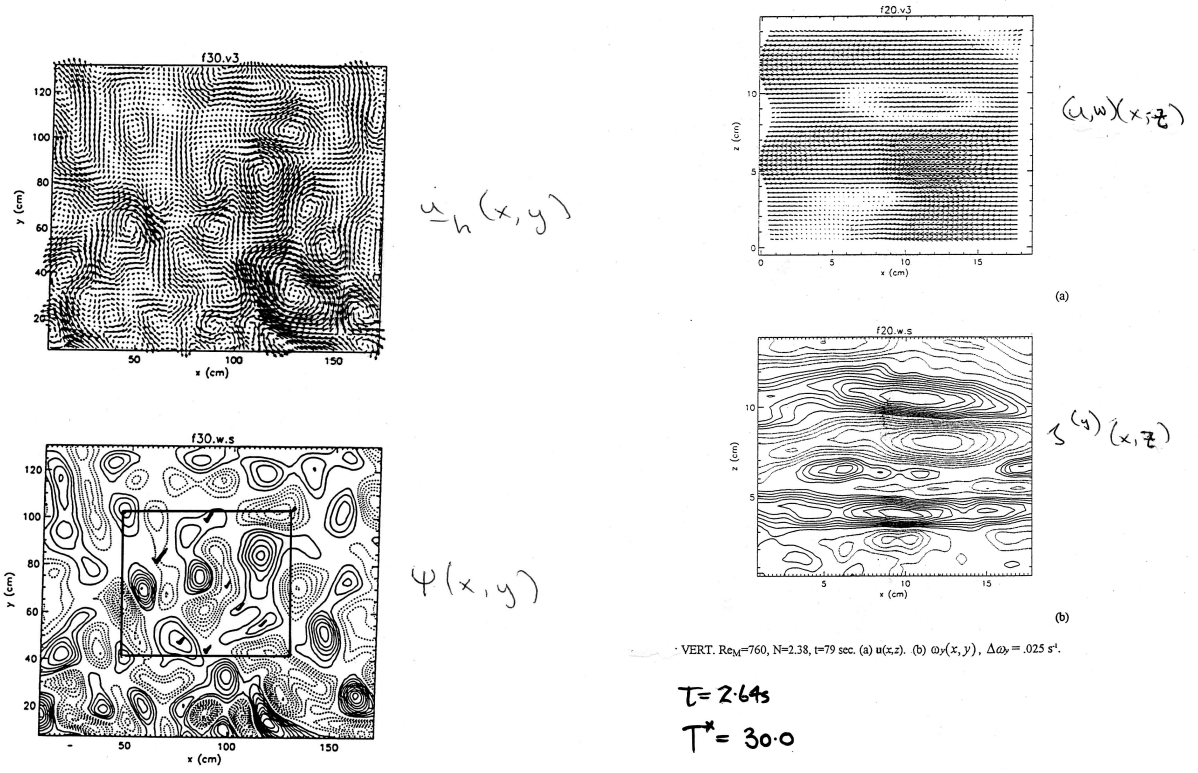

Figure 9: Spatial patterns: horizontal velocity and streamfunction in a horizontal plane (left two panels), horizontal velocity in a vertical plane (upper right), and the orthogonal component of horizontal vorticity in a vertical plane (lower right) in stably stratified turbulence for $Nt \gg 1$. Note the layers of high vertical shear. (Fincham *et al.*, 1996)

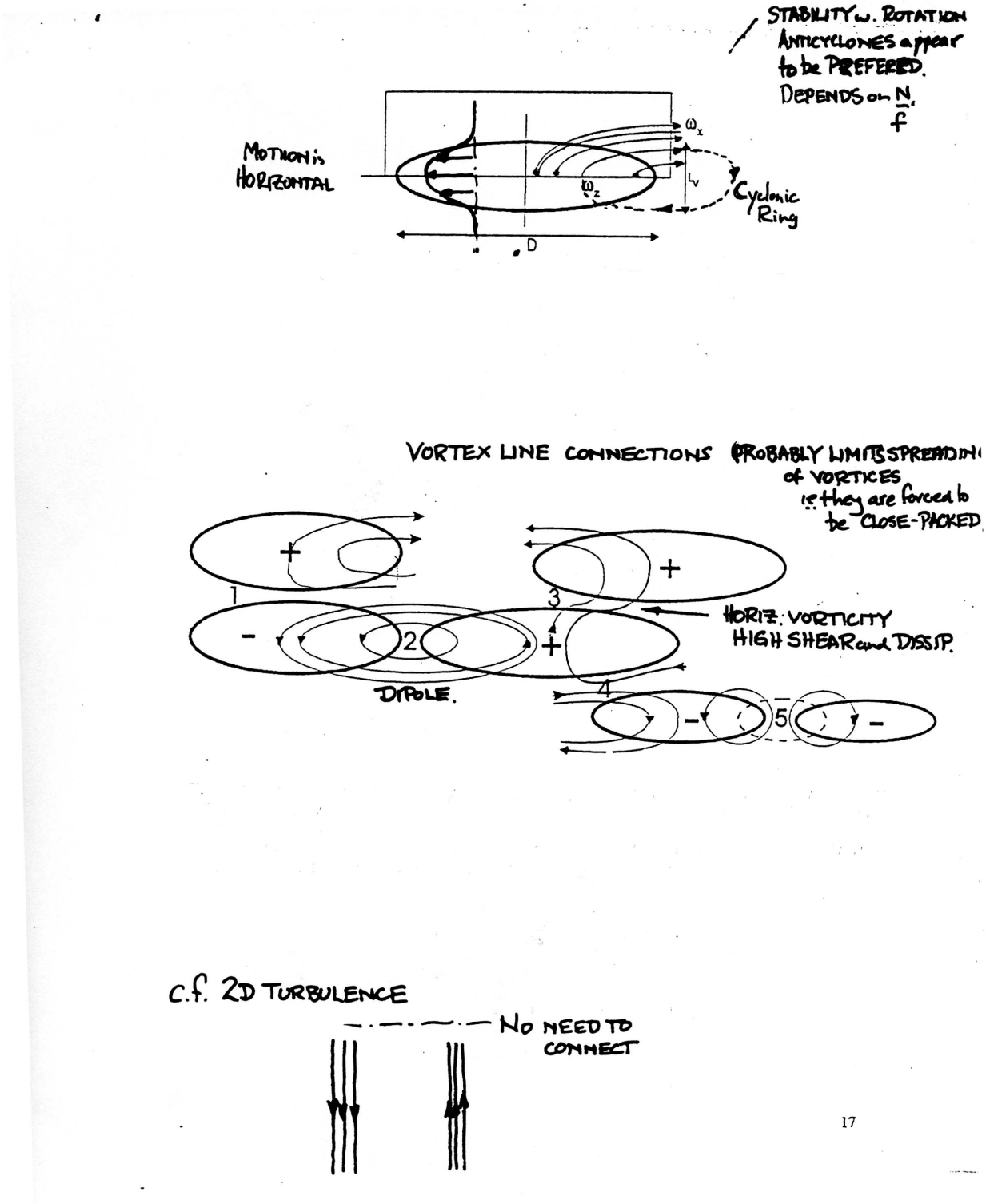

Figure 10: Sketches of the pancake vortex shape and vortex line geometry in stably stratified turbulence for $Nt \gg 1$. (Maxworthy, 1998)

- the Thorpe scale (here designated by L_T), which indicates the scale of vertical overturning motions (a.k.a. mixing length) as the minimal vertical parcel displacements such that an adiabatic rearrangement of an instantaneous density profile renders it marginally gravitationally stable (see Fig. 11, left panel).

- the Ozmidov scale $L_O = (\varepsilon/N^3)^{1/2}$, and its shear counterpart, the Corrsin scale $L_C = (\varepsilon/S^3)^{1/2}$, where N and S are the horizontally averaged buoyancy and shear frequencies.

- the Kolomogorov scale, $\eta = L_K = (\nu^3/\varepsilon)^{1/4}$.

In a typical stratified shear layer cycle (Fig. 11), we see that ℓ_θ grows monotonically but on slowly at very late time after the event is mostly over; L_T (and a closely related L_{T3}) and L_O and L_C all have a peak in the middle of the cycle when the turbulent mixing and cascade are strongest; L_T, L_{T3} are larger than L_O and L_C except at very late time, indicating that the cascades are significantly buoyancy influenced in the large eddies; and L_K shows a minimum in the middle and grows toward ℓ_θ at very late times as the turbulence decays away.

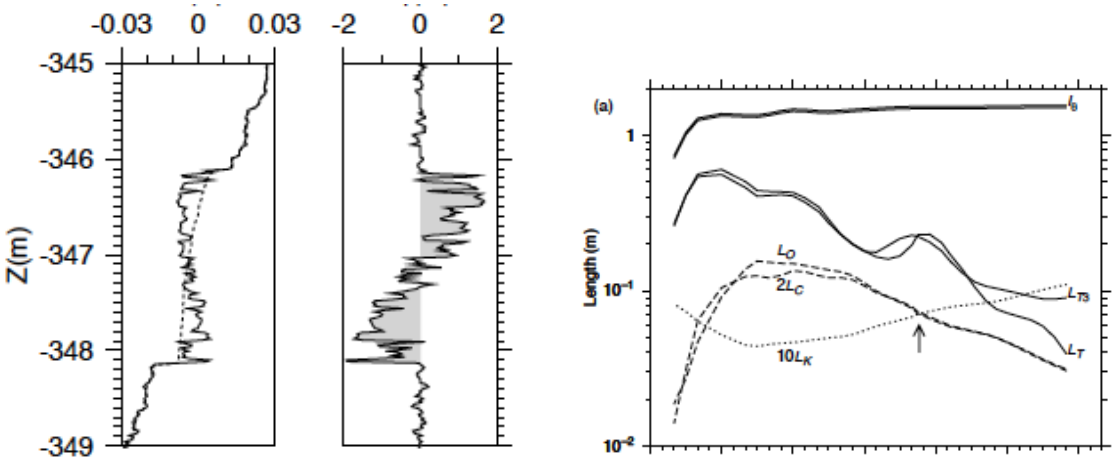

Figure 11: (Left) Illustration of the diagnosed Thorpe scale $L_T = d_T$ (right sub-panel) for an instantaneous a vertical profile of temperature T (left sub-panel), with the dashed line representing the rearranged profile. (Right) History of different vertical length scales defined in the text for a stratified shear layer with an instability-mixing-cascade life cycle. (Smyth and Moum, 2000)

5 Equilibrium Stratified Turbulence

Since stratified turbulence, like 3D homogeneous turbulence, is highly dissipative, it must be sustained by some sort of forcing on larger scales. In nature it is not rare for it to occur intermittently, suggesting that its forcing events may be sporadic. In contrast to the freely decaying and collapsing regimes in Secs. 2-3, now consider an equilibrium regime maintained by random, rotational forcing on scales much larger than L_O.

For small Fr and intermediate values of Re, the equilibrium behavior is consistent with the decaying behavior: Ri is small everywhere; ψ is $\gg \chi$; pancake vortices are the dominant flow

structure; and ε occurs mainly through the vertical shear variance. What happens as Re is increased further? Does the equilibrium energy level increase as balanced advective dynamics diminishes the efficiency of the forward energy cascade?

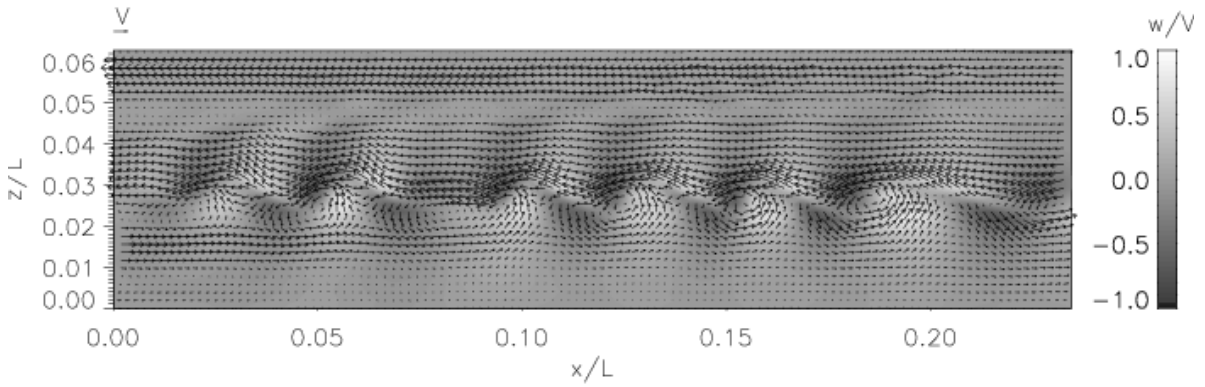

Figure 12: A local overturning event in a simulation of equilibrium stratified turbulence with random rotational forcing at large scales and $Re_\lambda = 1000$. Plotted are instantaneous vertical velocity (greyscale) and $(0, v, w)$ velocity (vectors) in a (y, z) plane; both are normalized by the r.m.s. velocity V indicated by the reference arrow in the upper left. L is the horizontal extent of the domain. (McWilliams, 2004)

In computational simulations Laval *et al.* (2003) show that there appears to be a boundary in (Fr, Re) space that distinguishes whether or not 2D and balanced breakdowns occur. When it does it primarily takes the form of local overturning motions in vertically thin layers, where the local Ri becomes small and the local buoyancy gradient may even become negative; the local flow patterns (Fig. 12) are quite similar to free shear layer and Kelvin-Helmholtz instabilities. This boundary is such that for any $Fr \ll 1$, breakdown events never occur for Re below some threshold value Re_c, but they do occur, at least infrequently, for larger $Re > Re_c$ (Figs. 13-14). By the requirement that $L_O \gg \eta$ as N increases for fixed ε, hence that ν decreases, it seems plausible that Re_c should increase as Fr decreases; *e.g.,* $Re_c \propto Fr^{-2}$ was suggested Riley and deBruynKops, 2003. This is not yet a fully explored behavior, in part because much of the laboratory work on stratified flow and all the previous computational work have been done with rather small values of Re.

In summary, for $Fr \ll 1$ there are stratified turbulent solutions to (5) that evolve self-consistently in time (*i.e.,* a Fr based on the outer scales of the turbulence remains small) on a characteristic advective evolution time of H/V, with relatively small w compared to $\mathbf{u}_h$ and small χ compared to ψ almost everywhere. Its leading order dynamical approximation is 2D flows in independent layers, but there are important dynamical corrections involving terms formally of $\mathcal{O}(Fr^2)$, many or most of which are probably consistent with the approximate dynamics contained in the Balance Equations. But at sufficiently high Re (*i.e.,* larger than some critical value, $Re_c \sim 5 \times 10^4$; Fig. 14), there also arise some local regions with Ri small or even negative, where overturning motions occur and the stratified turbulence cascade transfers energy into "unbalanced motions", more like internal gravity waves and/or Kolmogorov's isotropic cascade. Recently Lindborg (2006) has demonstrated a forward energy cascade inertial range, $E(k) \propto \varepsilon^{2/3} k^{-5/3}$, in simulations of

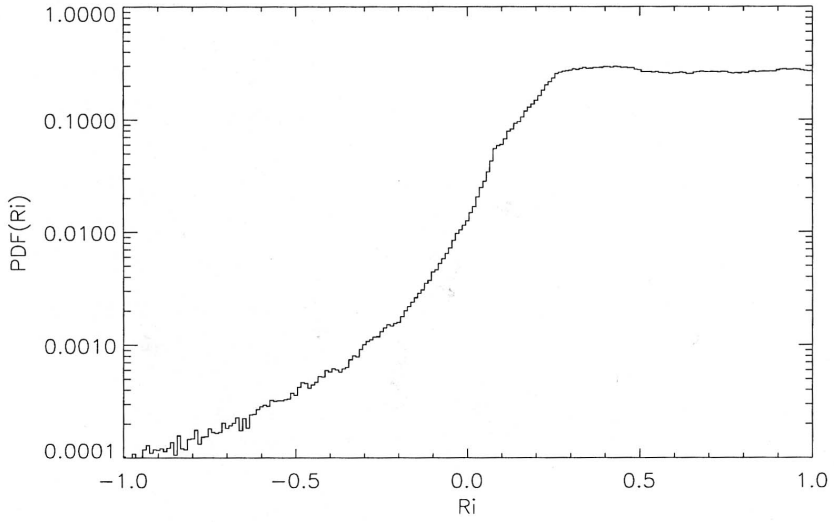

Figure 13: The PDF for local-gradient Ri values in equilibrium stratified turbulence with $Re_\lambda = 1000$. (An unpublished extension of Laval *et al.*, 2003)

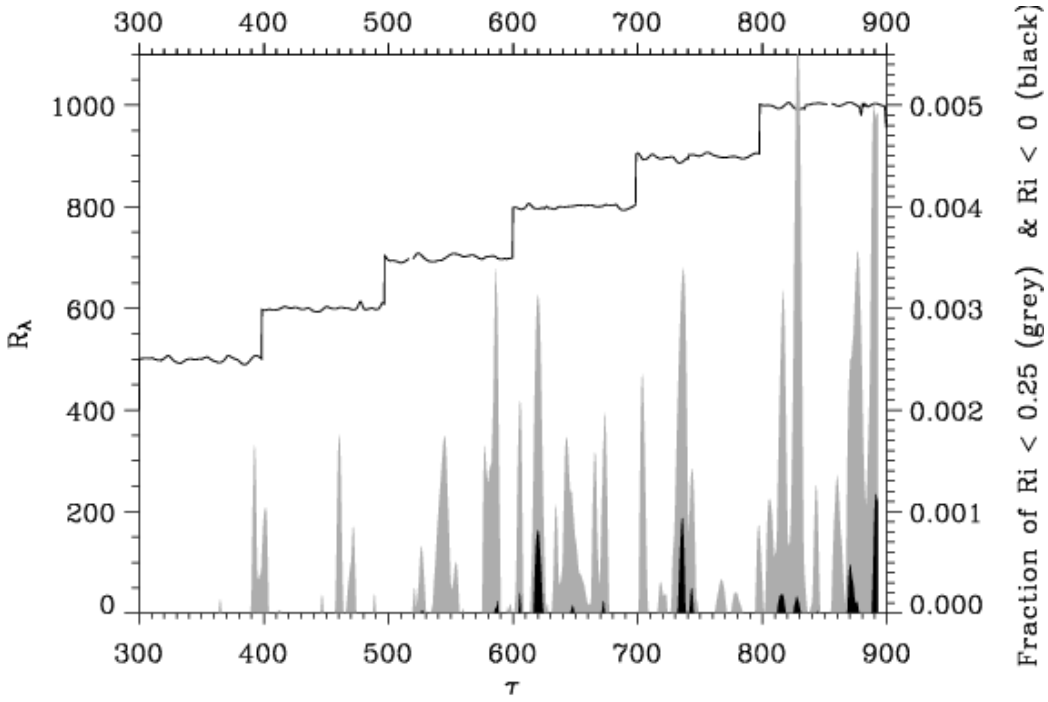

Figure 14: Experimental path in $Re_\lambda(t)$ (black line) for randomly forced stratified turbulence with fixed, small Fr value (≈ 0.08) and a step-wise decreasing viscosity $\nu(t)$ every $\Delta\tau = 100$. τ is a non-dimensional time normalized by the eddy turnover time. Between steps in ν the flow approximately comes into equilibrium with its forcing. Also shown are time series for the volume fraction of the domain with local $Ri < 0.25$ (filled gray area) and $Ri < 0$ (filled black area). There is no occurrence of $Ri < 0.25$ for $\tau \leq 300$ and $Re_\lambda \leq 500$, but small Ri values increase with increasing Re_λ values > 500. (Laval *et al.*, 2003; McWilliams, 2004)

randomly-forced equilibrium stratified turbulence with $Re > Re_c$ (Fig. 15)[3]. This is manifested in vertically layered structures with a local vertical scale, $H \sim V/N$, indicating a breakdown of the asymptotic scaling assumption of $Fr \ll 1$ uniformly in space and time. His solutions show that the flow remains anisotropic even at the largest Re values achieved, although it seems plausible that isotropy will the the eventual outcome on small enough scales, consistent with the validity of the H1 hypothesis (*3D Homogeneous Turbulence*).

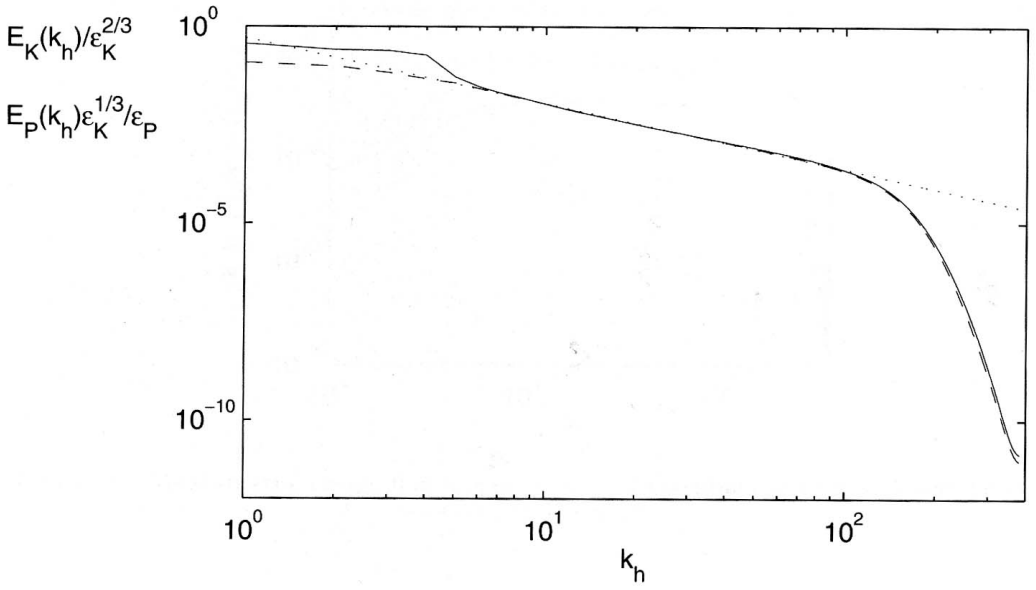

Figure 15: Normalized horizontal kinetic energy (solid line) and potential energy (dashed line) in a simulation of equilibrium, randomly forced, stratified turbulence. Note the well developed inertial range with $E \propto k^{-5/3}$ (dotted line). (Lindborg, 2006)

To better characterize this high Re regime with forward energy cascade, it is useful to define a horizontal Froude number, $F_h = V/fL$ that characterizes the spectrum peak flow in Fig. 15. This can be distinguished from the vertical Froude number used previously in these notes, *i.e.,* $F_v = Fr = V/NH$. The qausi-equilibrium, high-Re regime is characterized by the following parameter relations:

$$F_h \ll 1\,, \qquad F_v \sim 1\,, \qquad \eta \ll H \ll L\,, \qquad L_O \gg \eta\,, \qquad Re_b = \frac{\epsilon}{\nu N^2} \gg 1\,. \tag{14}$$

The last quantity is called the *buoyancy Reynolds number*, and its largeness is simply are reorganization of the $L_O \gg \eta$ relation. Figure 16 shows that Re_b is the most useful parameter to identify this regime with an energy inertial range, and Fig. 17 illustrates the flow in this regime (*n.b.,* this is a more fully developed turbulence pattern than the onset behavior shown in Fig. 12 for Re_b not as large).

[3]A companion study (Lindborg, 2005) shows that this behavior persists even in the presence of rotation until the Rossby number Ro drops below a critical $\mathcal{O}(1)$ value, where a transition is made to the inverse energy cascade of geostrophic turbulence.

In contrast and in terms of the same parameters, the "Lilly" regime of stratified turbulence with quasi-2D turbulence in independent vertical layers and/or "balanced" vortical motions, which applies to the laboratory experiments in Sec. 3 and earlier numerical simulations with smaller Re values, is characterized by

$$F_h \ll 1\,, \qquad F_v \ll 1\,, \qquad H \lesssim \eta \ll L\,, \qquad L_O \lesssim \eta\,, \qquad Re_b \lesssim 1\,. \tag{15}$$

Therefore, while the $k^{-5/3}$ mesoscale wind spectrum near the tropopause could be interpreted as the result of either an inverse or forward energy cascade in stratified turbulence, it now seems most likely that it is a forward range, fed in part by breakdown of geostrophic balance on larger scales (*Geostrophic Turbulence*). *I.e.,* it is now not very plausible that an inverse-cascading inertial range, analogous to 2D turbulence, is realizable in stratified turbulence in the ocean or atmosphere. Alternatively, the atmospheric mesoscale spectrum could be interpreted as mainly an inertia-gravity weak-wave turbulence, as some recent measurement analyses indicate, and this has long been the more comment view of currents in the oceanic interior on intermediate scales $\sim 0.05 - 10$ km.

6 Cox-Osborne Model

Geophysical measurements of turbulent velocity and buoyancy fluctuations on very small scales (often called "microstructure"), just larger than η, provide estimates of the local kinetic energy and buoyancy variance dissipation rates,

$$\varepsilon \;=\; \nu\overline{(\nabla \mathbf{u})^2} \;\;\text{and}\;\; \chi \;=\; 2\kappa\overline{(\nabla b)^2}\,, \tag{16}$$

with the average made over the microscale fluctuations (*i.e.,* on a scale larger than η). (Note that in this context χ is the buoyancy variance dissipation rate, not the divergent horizontal velocity potential in (6).) We consider approximate, local equilibrium forms for the TKE and $\overline{b^2}$ balance equations, neglecting all tendency and transport terms and considering only the turbulent production by the Reynolds stress work associated with the mean vertical shear and the analogous turbulent buoyancy variance generation as the sources balancing the sinks of the dissipation rates (Osborne and Cox, 1972):

$$\begin{aligned} \overline{\mathbf{u}_h' w'} \cdot \frac{\partial \overline{\mathbf{u}}_h}{\partial z} &= +\,\overline{b' w'} - \varepsilon \\ \overline{b' w'} N^2 &= -\,\frac{1}{2}\chi\,. \end{aligned} \tag{17}$$

In these equations, we can insert the eddy-viscosity and eddy-diffusivity definitions in place of the turbulent fluxes,

$$\nu_e \;=\; -\overline{\mathbf{u}_h' w'} \Big/ \frac{\partial \overline{\mathbf{u}}_h}{\partial z} \;\;\text{and}\;\; \kappa_e \;=\; -\overline{b' w'} \Big/ N^2\,. \tag{18}$$

This yields a pair of coupled equations for the eddy diffusivities in terms of the measured mean-field gradients and dissipation rates:

$$\begin{aligned} \nu_e \left(\frac{\partial \overline{\mathbf{u}}_h}{\partial z} \right)^2 &= \frac{\chi}{2N^2} + \varepsilon \\ \kappa_e N^4 &= \frac{1}{2}\chi\,. \end{aligned} \tag{19}$$

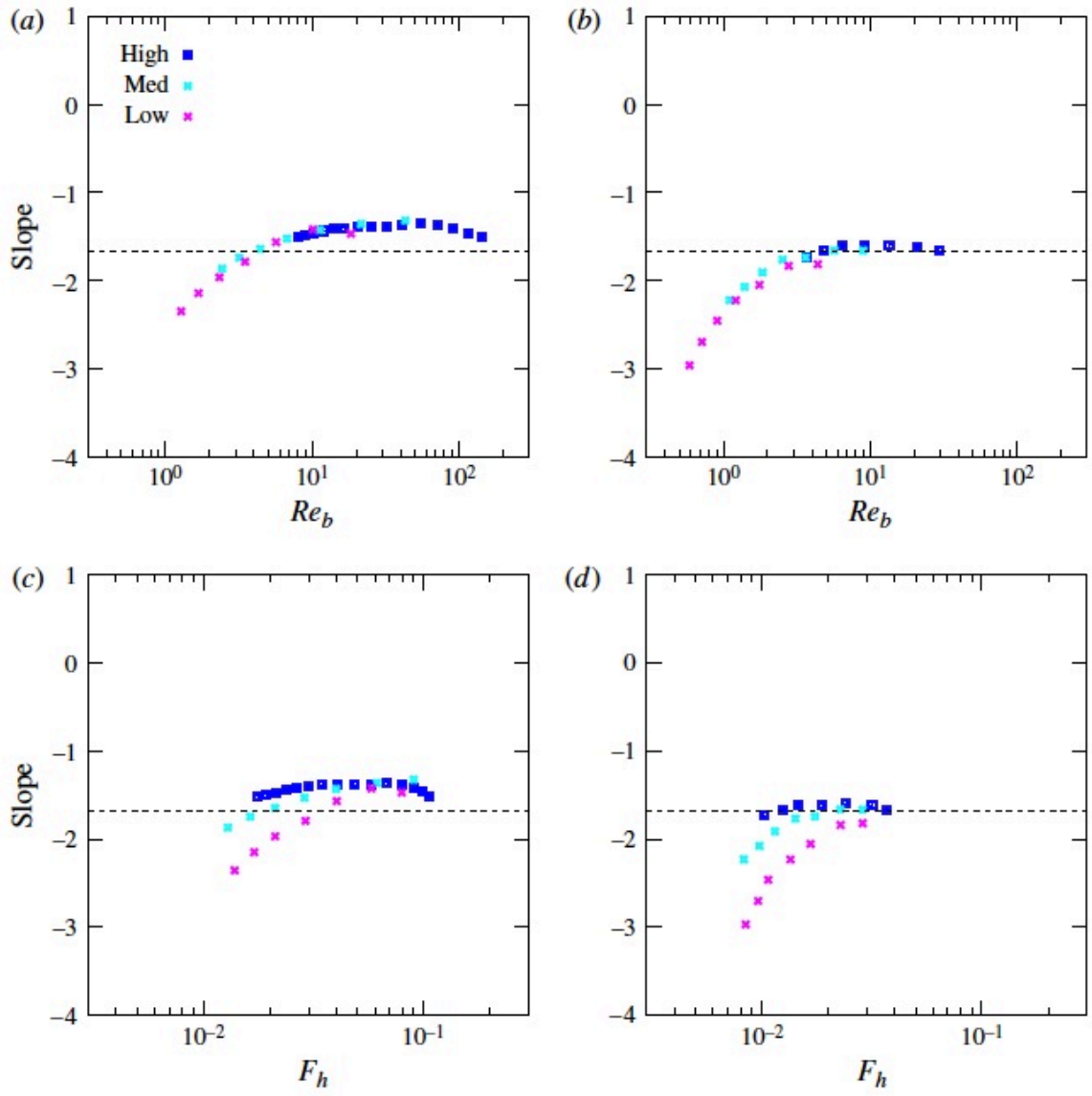

Figure 16: The slopes of the horizontal wavenumber spectrum of the horizontal kinetic energy velocity in simulations of freely decaying stratified turbulence for times after the time of maximum enstrophy. They are plotted either as a function of Re_b (a,b) or as a function of the horizontal Froude number $F_h = V/NL$. The value of N is twice as large in (a,c) as in (b,d). High, Medium, and Low cases refer to the initial Reynolds numbers, $Re = VL/\nu \gg 1$. This shows that, for large Re_b and small Fr_h (*i.e.,* the (14) regime), the $k_h^{-5/3}$ inertial range slope is achieved, but Re_b is a more successful control paratmeter than F_h in organizing these multiple cases. (Bartello and Tobias, 2013)

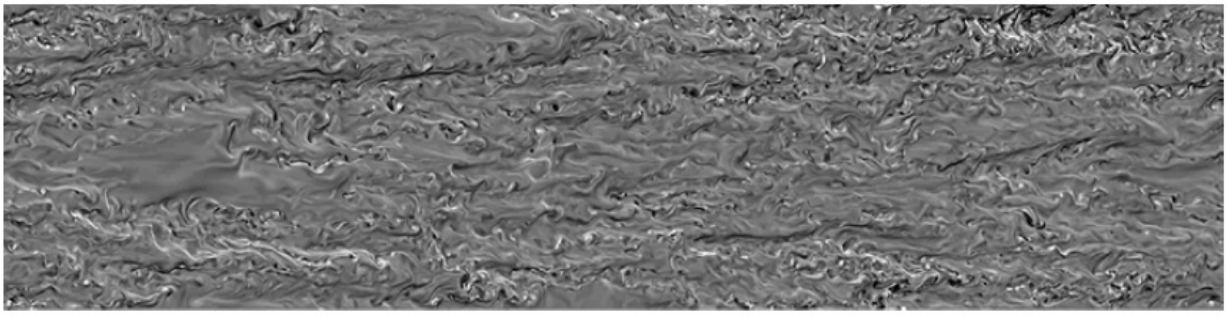

Figure 17: Snapshot of the component of the horizontal vorticity perpendicular to the page for the larger N case at the highest Reynolds number at a time when $Re_b \approx 6.5$ for the simulations in Fig. 16. Notice the vertical layers and local overturns. (Bartello and Tobias, 2013)

Thus, in a stably stratified fluid with positive eddy transfer coefficients, turbulence generation is entirely by shear production, and it is balanced by the sum of the kinetic energy and buoyancy-variance dissipation rates. For $Fr < 1$, ε is typically larger than χ/N^2. A common assumption, with considerable empirical support, is that the *flux Richardson number*,

$$\begin{aligned} Ri_f &\equiv \overline{b'w'}\Big/\overline{\mathbf{u}_h'w'}\cdot\frac{\partial\overline{\mathbf{u}}_h}{\partial z} \\ &= \kappa_e N^2\Big/\nu_e\left(\frac{\partial\overline{\mathbf{u}}_h}{\partial z}\right)^2 \quad [\sim 1\Big/Pr_e Fr^2\,] \\ &= \chi/2N^2\big/(\chi/2N^2+\varepsilon)\,, \end{aligned} \tag{20}$$

has been determined empirically to have a typical value of about 0.15, hence

$$\frac{\chi}{2} \approx \Gamma\varepsilon N^2 \quad \text{and} \quad \kappa_e \approx \Gamma\varepsilon/N^2 \tag{21}$$

for $\Gamma = Ri_f/(1-Ri_f) \approx 0.2$, the so-called *mixing efficiency* (Toole, 1998). The *eddy Prandtl number* in (20) is defined analogously to the molecular one, $Pr_e = \nu_e/\kappa_e$.

Another common assumption is that the flow is statistically isotropic near the Kolmogorov scale (*i.e.,* the H1 hypothesis); with this further assumption, then we can estimate ε and χ by the following formulas[4]:

$$\varepsilon = \frac{15}{4}\nu\overline{\left(\frac{\partial\mathbf{u}_h'}{\partial z}\right)^2} \quad \text{and} \quad \chi = 6\kappa\overline{\left(\frac{\partial T'}{\partial z}\right)^2}\,. \tag{22}$$

The end result is a procedure for estimating dissipation rates and eddy diffusivities from fine-scale vertical profiles of b (or often just T) and $\mathbf{u}_h$. It rests on assumptions of local production-dissipation and isotropy that seem solid for shear turbulence with $Fr = \mathcal{O}(1)$ and are still somewhat uncertain for $Fr \ll 1$.

[4]The prefactor for ε depends upon the distinction between longitudinal and transverse shear variances, with the former half as large as the latter (Batchelor, 1953). The general expression in (16) is comprised of 6 transverse shear variance components and 3 longitudinal ones, implying that ε proportionality factor for a single transverse shear variance component is $6 + 3/2 = 15/2$ (and half this for the two components in (22)).

7 Oceanic Microstructure and Diapycnal Mixing

The approach in Sec. 6 is often referred to as *microstructure* estimates of the turbulent transport rates. It was proposed by Osborn and Cox (1972) in the oceanic context, although there are earlier precedents in engineering-turbulence second-moment modeling. It has been used extensively to survey geophysical turbulence, particularly in the upper ocean. An example of this approach is shown in Figs. 18-19 for the upper equatorial ocean. This is a region containing some strong vertical shears associated with the Equatorial Undercurrent. (Another place small Ri can be found is near the Jet Stream, where *clear-air turbulence* occurs.) The eddy coefficients inferred from (19) are plotted against Ri. They are much larger for stratified shear turbulence, with $0 \leq Ri \leq 0.25$ (note that $\tan^{-1}(0.25) = 0.5$), than for more strongly stably stratified turbulence, with $Ri > 0.25$. Even in the latter case, however, the eddy diffusivities are larger than their molecular counterparts by more than an order of magnitude. Notice also that $\nu_e \gg \kappa_e$ in the stratified regime, whereas $\nu_e \approx \kappa_e$ for small Ri; *i.e.,* the eddy Prandtl number Pr_e is large for stratified turbulence and $\mathcal{O}(1)$ for shear turbulence. Even within the stratified turbulence regime, the eddy diffusivities appear to decrease as Ri increases, albeit only slowly.

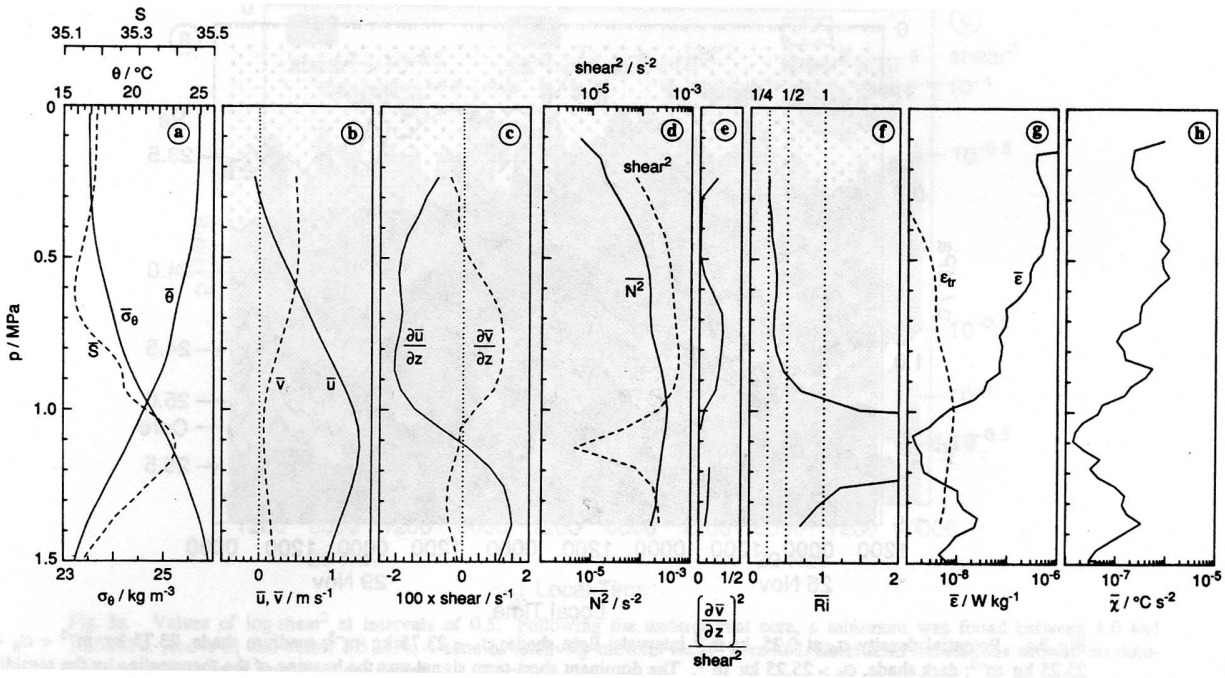

Figure 18: Average vertical profiles from a 4.5 day oceanic time series at the Equator. Pressure is in MPa (≈ 100 m). (Peters *et al.*, 1988)

Thus, the vertical turbulent fluxes in stably stratified interior regions of the ocean and atmosphere are usually rather small; nevertheless, they can be significant if no other transport process is more efficient. The oceanic pycnocline and the atmospheric stratosphere are two places where this is often so.

Figures 20-21 are taken from a zonal-vertical section across the Gulf Stream (Fig. 20a) where it passes through the Florida Strait. The stratification (*n.b.,* Fig. 20b, for the potential density,

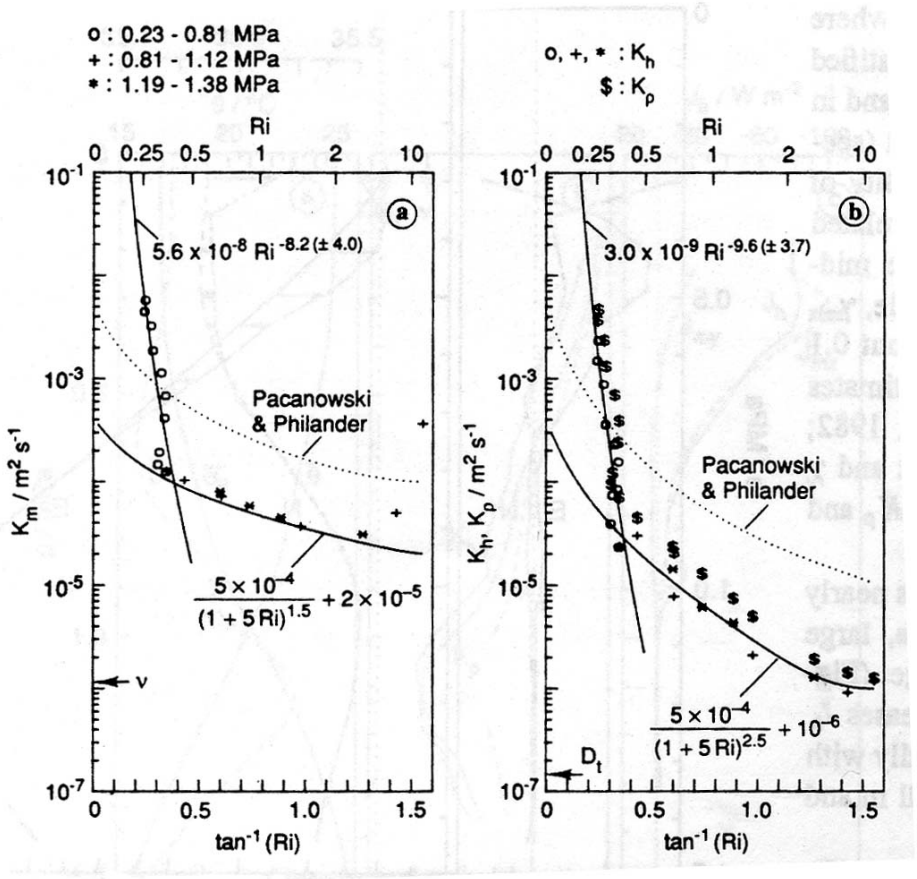

Figure 19: Eddy diffusion coefficients for momentum, heat, and density as functions of "mean" Ri from the 4.5 day oceanic time series on the equator. For comparison a parameterization by Pacanowski and Philander (1981) is plotted. (Peters *et al.*, 1988)

$\sigma_\theta = \rho_\theta - 10^3$ kg m^{-3}) is small in the surface boundary layer of less than 50 m (*i.e.,* ≈ 0.5 MPa, in pressure units) thickness, large in the pycnocline reaching down to about 300 m, and again rather small in the deeper water. Because of the strong mean current, Fr (based on density and velocity gradients over $\Delta z = 10$ m) in Fig. 20c is not extremely large anywhere. Nevertheless in Fig. 20d, κ_b from (21) is much smaller in the vertical interior than it is in the top and bottom boundary layers, especially so in the pycnocline. This is also seen in Fig. 21a for profiles averaged over many samples. Very near the bottom (Fig. 21b), the density and current profiles are well mixed over the bottom boundary layer of about 40 m thickness, but the depth interval, with ε much larger than in the interior, spans not only the bottom boundary layer but also the 50 m thick stratified shear layer above it.

The most common present interpretation of mixing in the oceanic interior is that internal waves are generated by flow over bottom topography, propagate upwards, and supply mixing energy to a layer of stratified turbulence above the boundary layer, presumably through local "breaking" events (Gregg, 1989). However, the formula (21) for κ_e is equally applicable to flows with a flux of energy ε from larger scales by a forward energy cascade (*e.g.,* stratified turbulence or even geostrophic turbulence if the geostrophic balance constraint breaks down). This predicted form for κ_e has recently been confirmed in stratified-turbulence simulations (Brethower and Lindborg, 2008). Thus, as with the open issue about the mix of internal waves and vortical motions in atmospheric and oceanic flows (Sec. 2), so too is the mix of sources for ε and diapycnal mixing not yet well known.

Figure 22 shows a compendium of $\kappa_e(z)$ profiles from various locations. Figure 22a shows what is believed to be the more widespread situation, with the smallest values in the pycnocline and somewhat larger values below, and Fig. 22b shows examples of "hot spots" where the turbulent mixing is unusually high due to either strong local mean shears or topographic features presumed to energize the internal wave field causing local breaking. Overall, the statistics and regime geographies of shear and stratified turbulence in the interior of the atmosphere and ocean are still only partly known.

The Thorpe scale (Sec. 4) is often analyzed in microstructure measurements because it too is calculable directly from individual profiles of buoyancy.

Continuing with abyssal oceanic mixing in "hot spots", a very recent observational example is van Haren *et al.* (2014). This ones comes from the poleward flow of Antarctic Bottom Water in the Tropical Atlantic, where the rough topography of the mid-Atlantic ridge forces the flow across a sill about 50 m high into a narrow valley about 7 km wide. The background stratification and velocity profiles on top and just past the sill are shown in Fig. 23: there is a strong horizontal flow and vertical shear in a stably stratified layer whose Ri value is near the marginal value for Kelvin-Helmholtz instability.

As thus anticipated, Kelvin-Helmholtz "billows" do arise (Fig. 24). They have a period of more than an hour, and their occurrence is modulated by the phase of the tidal current, which brings the local Ri value down to around Ru_{cr} and induces large-amplitude billows in θ. There is also a tidal oscillation in the strength of the energy dissipation ε and the corresponding diapycnal eddy diffusivity κ_ρ that peaks with large values of $> 10^{-6}$ m^2 s^{-3} and $> 10^{-2}$ m^2 s^{-1}, respectively. The latter is larger than any of the values shown in Figs. 20- 22, except for the Strait of Gibraltar, where the same mechanism of Kelvin-Helmholtz instability is known to occur (Fig. 25).

Thus, in this particular location a clear mechanism for highly elevated diapycnal mixing has been identified. Strictly speaking it is not a pure case of stratified turbulence because it occurs on

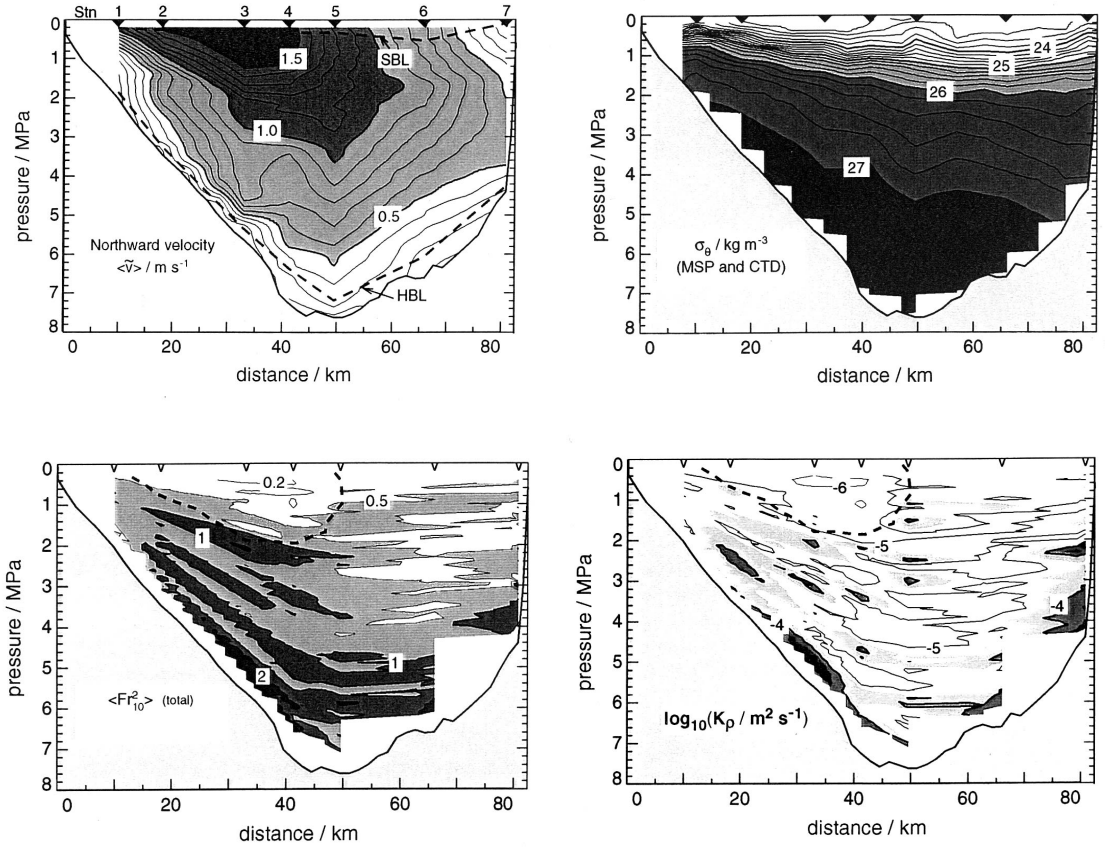

Figure 20: Measurements of velocity (upper left), potential density (upper right), averaged Froude number computed with 10 m vertical differences (lower left), and eddy diffusivity for density, K_ρ (lower right), across the Florida Strait. The vertical coordinate is pressure, with 1 MPa $\approx$ 100 m depth. (Gregg *et al.*, 1999)

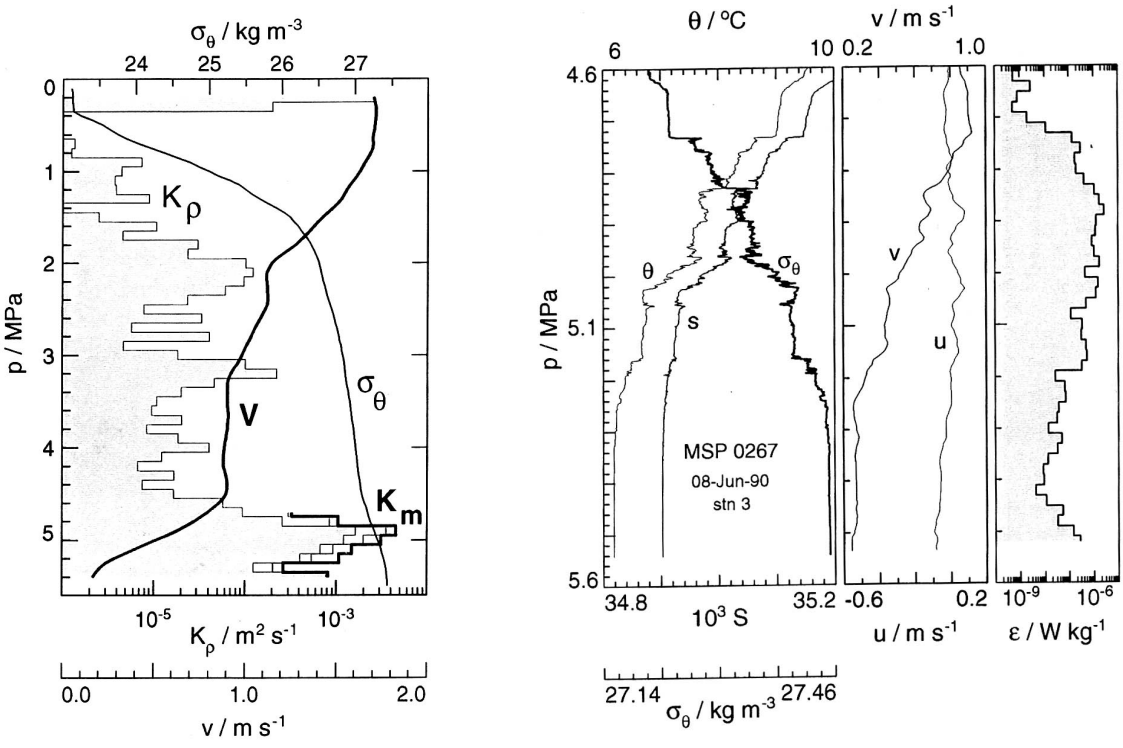

Figure 21: Microstructure profiles in the Florida Strait: through the core of the Gulf Stream (left) and near the bottom boundary layer (right). (Gregg *et al.*, 1999)

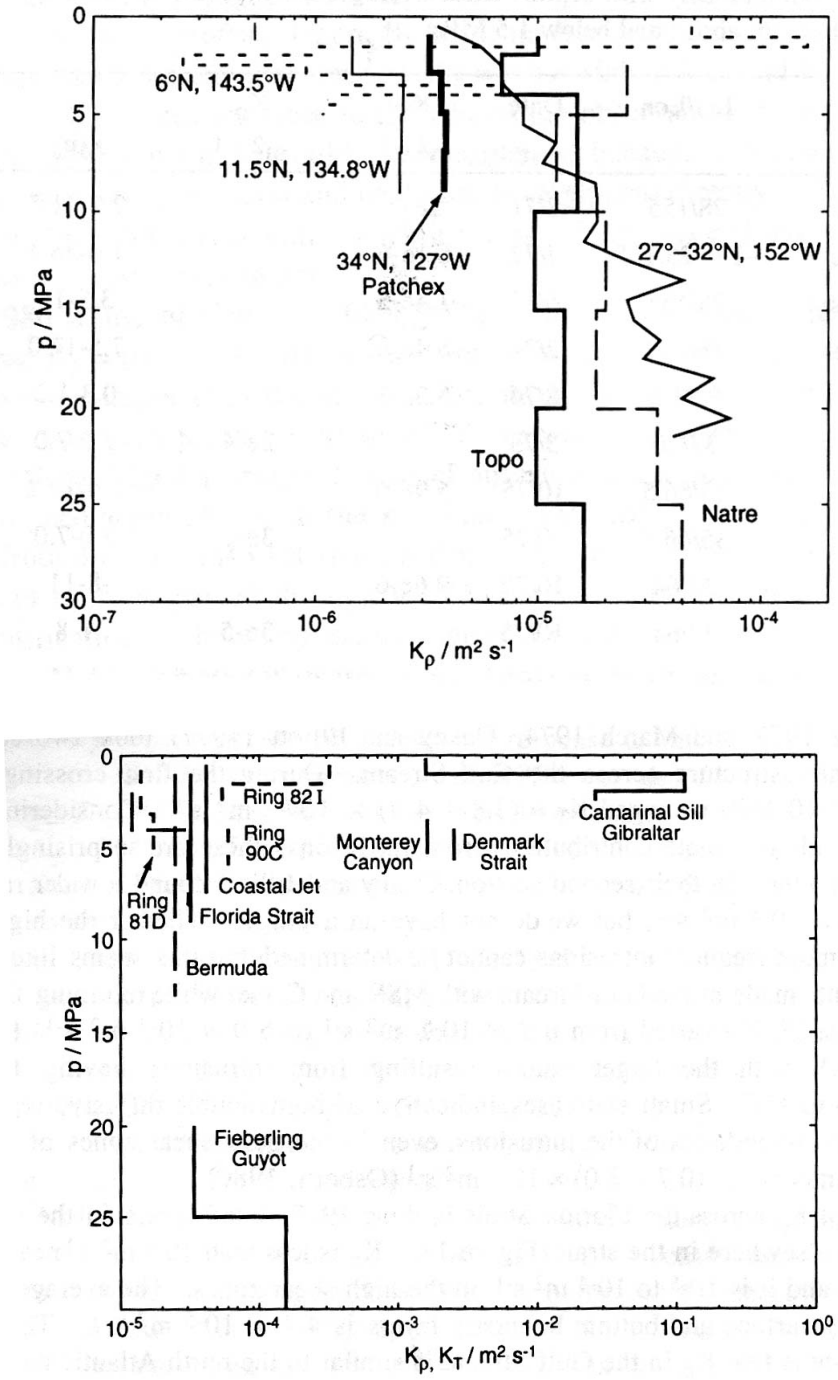

Figure 22: Estimates of diapycnal κ_ρ: (Top) regions not known to be influenced by strong topography or mesoscale currents, and (Bottom) regions suspected of being mixing hot spots including fronts, strong mesoscale eddies, islands, seamounts, straits, and canyons. (Gregg, 1998)

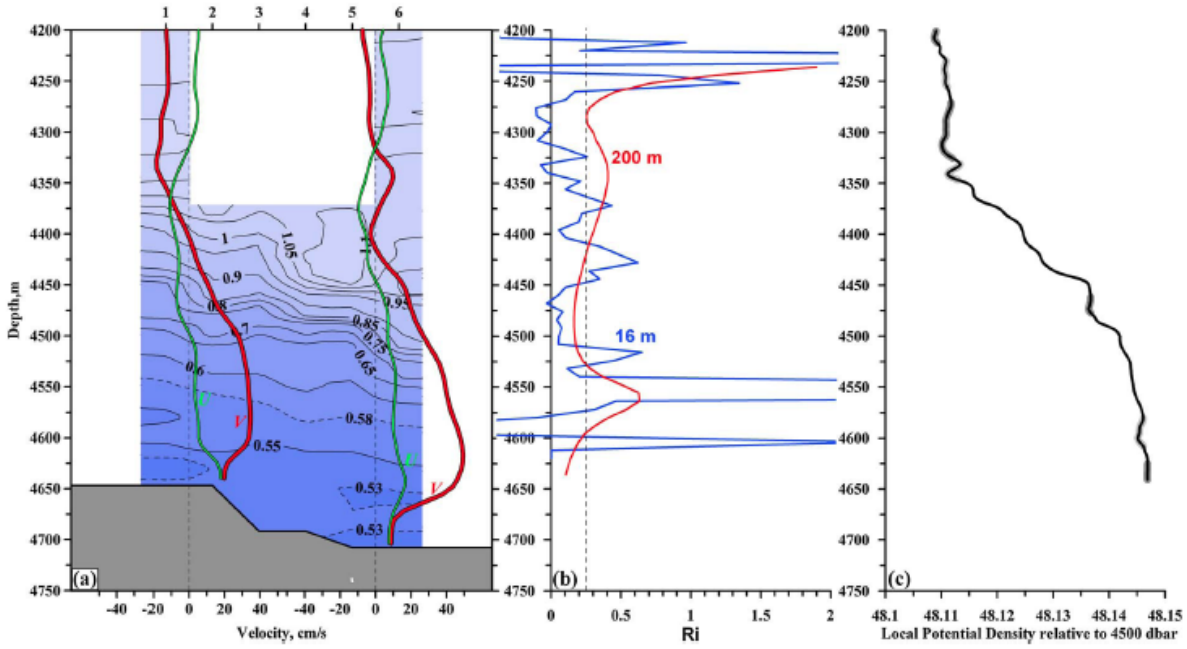

Figure 23: Background vertical profiles of (a) currents and temperature, (b) gradient Ri from "raw", $\Delta z = 16$ m and "smoothed, $\Delta z = 200$ m vertical intervals, and (c) potential density anomaly with respect to a reference pressure of 4500 dB (= m) depth. The vertical line in (b) indicates a critical value of $Ri_{cr} = 0.25$. (van Haren *et al.*, 2014)

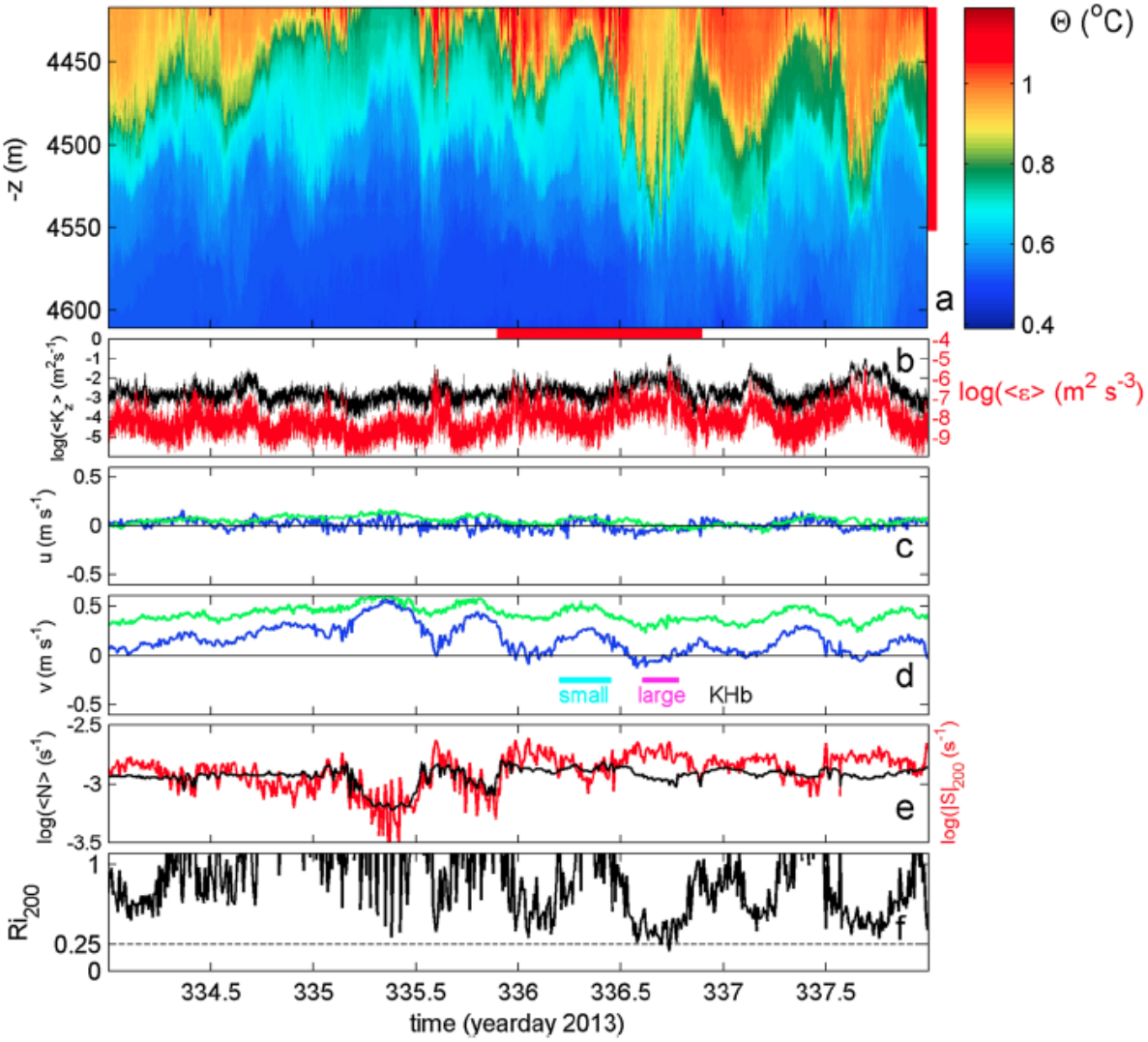

Figure 24: Four-day sample of moored observations: (a) depth-time series of potential temperature θ, (b) time series of vertically averaged ($\Delta z = 200$ m) kinetic energy dissipation rate ε (red) and eddy diffusivity $\kappa_z = \kappa_\rho$ (black), (c) zonal velocity from upper (blue) and lower (green) current meter, (d) same for meridional velocity, (e) $\log[N]$ and $\log[\partial_z v]$ computed with $\Delta z = 200$ m, and (f) Ri from quantities in (e). (van Haren *et al.*, 2014)

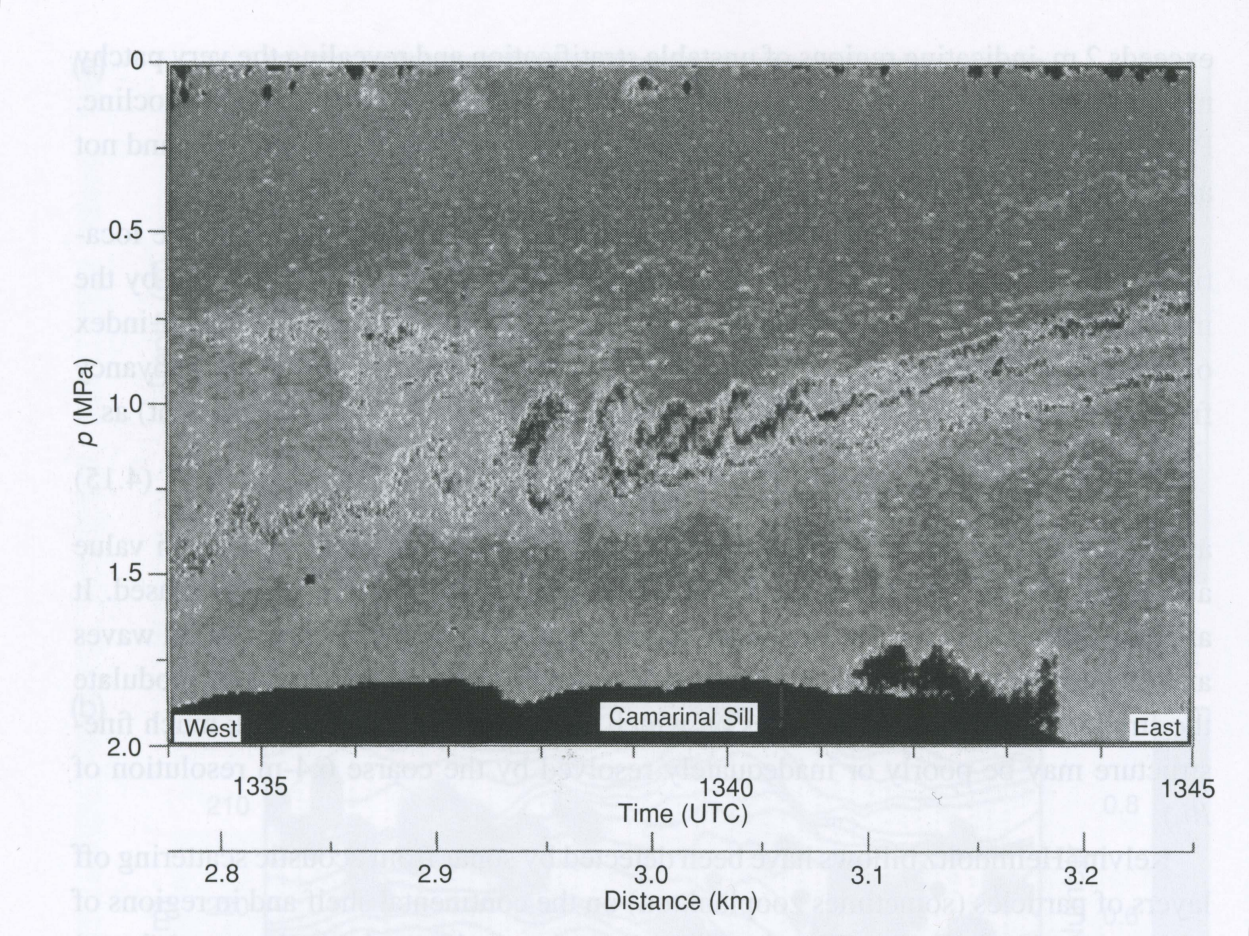

Figure 25: Kelvin-Helmholtz billows in the Strait of Gibraltar. The larger billows are about 25 m high around 125 m depth ($p = 1.25$ MPa). The background flow is eastward above and westward below with stable stratification, typical of the evaporation-driven exchange flow between the Atlantic and Mediterranean. (Thorpe, 2007)

the margin of stratification dominance, *i.e.,* its Fr value sometimes is not small. For most of the oceanic and atmospheric interiors, however, the typical Fr values are small, and on smaller scales of 0.5-5 km or so, the dynamics are a mixture of internal gravity waves and stratified turbulence.

References

Bartello, P., and S. Tobias, 2013: Sensitivity of stratified turbulence to the buoyancy Reynolds number. *J. Fluid. Mech.* **725**, 1-22.

Batchelor, G.K., 1953: *The Theory of Homogeneous Turbulence*. Cambridge.

Brethouwer, G., and E. Lindborg, 2008: Numerical study of vertical dispersion by stratified turbulence. *J. Fluid Mech.*, in press.

Fincham, A.M., T. Maxworthy, and G.R. Spedding, 1996: Energy dissipation and vortex structure in freely decaying, stratified grid turbulence. *Dyn. Atmos. Oceans* **23**, 155-169.

Gregg, M.C., 1989: Scaling turbulent dissipation in the thermocline. *J. Geophys. Res.* **94**, 9686-9698.

Gregg, M.C., 1998: Estimation and geography of diapycnal mixing in the stratified ocean. *Physical Processes in Lakes and Oceans. Coastal and Estuarine Studies* **54**, 305-338.

Gregg, M.C., D.W. Windel, J.A. MacKinnon, and R.C. Lien, 1999: Mixing on shelves and slopes. In: *Proceedings of 'Aha Huliko'a Winter Workshop*, P. Müller (ed.), University of Hawaii.

van Haren, H., L. Gostiaux, E. Morozov, and R. Taraknov, 2014: Extremely long Kelvin-Helmholtz billow trains in the Romanch Fracture Zone. *Geophys. Res. Lett.* **41**, 8445-8451.

Laval, J.P., J.C. McWilliams, & B. Dubrulle, 2003: Forced stratified turbulence: Successive transitions with Reynolds number. *Phys. Rev. E* **68**, 036308/1-036308/8.

Lilly, D., 1983: Stratified turbulence and the mesoscale variability of the atmosphere. *J. Atmos. Sci.* **40**, 749-761.

Lin, J.T., and Y.H. Pao, 1979: Wakes in stratified fluids. *Ann. Rev. Fluid Mech.* **11**, 317-338.

Lindborg, E., 2006: The energy cascade in a strongly stratified fluid. *J. Fluid Mech.* **550**, 207-242.

Lindborg, E., 2005: The effect of rotation on the mesoscale energy cascade in the free atmosphere. *Geophys. Res. Lett.* **32**, L01809-1 – L01809-4.

Majda, A.J., and M.J. Grote, 1997: Model dynamics and vertical collapse in decaying strongly stratified flows. *Physics of Fluids* **9**, 2932-2940.

Métais, O., and J.R. Herring, 1989: Numerical simulations of freely evolving turbulence in stably stratified fluids. *J. Fluid Mech.* **202**, 117-148.

Maxworthy, T., 1998: *The Role of Laboratory Experiments in Physical Oceanography: A Review*. From a lecture.

McWilliams, J.C., 1985: A note on a uniformly valid model spanning the regimes of geostrophic and isotropic, stratified turbulence: Balanced turbulence. *J. Atmos. Sci.* **42**, 1773-1774.

McWilliams, J.C., I. Yavneh, M.J.P. Cullen, and P.R. Gent, 1998: The breakdown of large-scale flows in rotating, stratified fluids. *Phys. Fluids* **10**, 3178-3184.

McWilliams, J.C., 2004: J.C., Phenomenological hunts in two-dimensional and stably stratified turbulence. In: *Atmospheric Turbulence and Mesoscale Meteorology: Scientific Research Inspired by Doug Lilly*. Eds. E. Fedorovich, B. Stevens, & R. Rotunno, Cambridge University Press, Cambridge, 35-49.

Osborn, T., and C. Cox, 1972: Oceanic finestructure. *Geophys. Fluid Dyn.* **3**, 321-345.

Pacanowski, R.C., and S.G.H. Philander, 1981: Parameterization of vertical mixing in numerical models of tropical oceans. *J. Phys. Ocean.* **11**, 1443-1451.

Peters, H., M.C. Gregg, and J.M. Toole, 1988: On the parameterization of equatorial turbulence. *J. Geophys. Res.* **93**, 1199-1218.

Riley, J.J., and S.M. deBruynKops, 2003: Dynamics of turbulence strongly influenced by buoyancy. *Phys. Fluids* **15**, 1-13.

Smyth, W.D., and J.N. Moum, 2000: Length scales of turbulence in stably stratified mixing layers. *Phys. Fluids* **12**, 1327-1342.

Stillinger, D.C., K.N. Helland, and C.W. Van Atta, 1983: Experiments on the transition of homogeneous turbulence to internal waves in a stratified fluid. *J. Fluid Mech.* **131**, 91-122.

Thorpe, S., 2007: *An Introduction to Ocean Turbulence*. Cambridge Press.

Toole, J., 1998: Turbulent mixing in the ocean. In: *Oceanic Modeling and Parameterization*, E. Chassignet & J. Verron, eds., NATO Science Series **C 516**, Kluwer Acad. Pubs., 171-189.